Spring 2021

Reconstructing Surface Water Carbonate Ion Concentration Changes in the Eastern Equatorial Pacific Across Glacial Transitions

Lenzie Gail Ward
Old Dominion University, lenzieward@gmail.com

RECONSTRUCTING SURFACE WATER CARBONATE ION CONCENTRATION CHANGES IN THE EASTERN EQUATORIAL PACIFIC ACROSS GLACIAL TRANSITIONS

by

Lenzie Gail Ward
B.S. May 2019, Old Dominion University

A Thesis Submitted to the Faculty of
Old Dominion University in Partial Fulfillment of the
Requirements for the Degree of

MASTER OF SCIENCE

OCEAN AND EARTH SCIENCES

OLD DOMINION UNIVERSITY
May 2021

Approved by:

Matthew W. Schmidt (Director)

Alexander Bochdansky (Member)

Margaret Mulholland (Member)

ABSTRACT

RECONSTRUCTING SURFACE WATER CARBONATE ION CONCENTRATION CHANGES IN THE EASTERN EQUATORIAL PACIFIC ACROSS GLACIAL TRANSITIONS

Lenzie Gail Ward
Old Dominion University, 2021
Director: Dr. Matthew W. Schmidt

Today, the eastern equatorial Pacific (EEP) plays a critical role in the global CO_2 budget as a major source of CO_2 to the atmosphere, but recent studies suggest the region may shift to a sink for atmospheric CO_2 under different climate states. Here, I focus on two transitional periods, the last deglaciation (25 kyr to present) and last glaciation (the Marine Isotope Stage (MIS) 5a-4 transition, 96 to 60 kyr), to investigate how the carbon system in the EEP responds to major climate changes. I measured B/Ca ratios in the planktic foraminifera *Globigerina bulloides* from core MV1014-17JC (00º10.83'S, 85º52.00'W; 2846 m water depth) as a proxy for changes in surface water carbonate ion concentration ($[CO_3^{2-}]$) in the EEP across both climate transitions. Because calcification rate (controlled by $[CO_3^{2-}]$) drives the uptake of boron in foraminiferal tests, $[CO_3^{2-}]$ can be calculated from B/Ca ratios. In addition to the B/Ca proxy, the relationship between $\delta^{13}C$ values in the planktic foraminifera *Globigerinoides ruber* and *Trilobatus sacculifer* to surface water $[CO_3^{2-}]$ differ in response to changes in seawater $[CO_3^{2-}]$. Therefore, I also measured $\delta^{13}C$ in these two species as another proxy for surface water $\Delta[CO_3^{2-}]$ change. Because surface water $[CO_3^{2-}]$ is linked to surface water CO_2 concentrations and thus atmospheric pCO_2, I use reconstructed $[CO_3^{2-}]$ to indicate if the EEP was more or less of a source of CO_2 to the atmosphere in the past. Results indicate that across both the deglaciation and glaciation, the EEP remained as much or more of a source of CO_2 than today. Enhanced upwelling across these

glacial transitions coupled with an expansion of the oxygen minimum zone (OMZ) likely delivered CO_2- and nutrient-rich water to the surface. However, this increase in nutrient concentrations coupled with dust fertilization across cold Heinrich events failed to stimulate biological productivity to the point where the region switched to being a sink for atmospheric CO_2. Sustained lower-than-modern surface water [CO_3^{2-}] across both climate transitions indicate that the EEP may remain a source of CO_2 to the atmosphere across anthropogenic climate changes in the future.

This thesis is dedicated to Nicholas.
Ah, yes, I see.

ACKNOWLDGEMENTS

Firstly, I thank my advisor, Dr. Matthew Schmidt for providing me with the opportunity to conduct this research, for teaching and guiding me, and for making me into a junior scientist. I also thank him to for trusting in my capabilities but also for thinking I am smarter than I really am. It keeps me on my toes. Next, I would like to thank Dr. Jennifer Hertzberg, my mentor, supporter, and friend. Your knowledge and skills never cease to amaze me. None of this could have ever been done without you. Thank you, Bettina Sohst, for your unbelievable ICP-MS skills and to Ryan Glaubke, Brian Close, and Colton Watkins for your company and help in and outside the lab. I would also like to thank my committee members, Dr. Alexander Bochdansky and Dr. Margaret Mulholland for their help and guidance. In addition, thank you to the Perry Honors College at Old Dominion University and the Neil and Susan Kelley family for research funding. I also must acknowledge my collaborators, Dr. Howie Spero and Dr. Franco Marcantonio for your roles in this project. To my support network, my sisters and friends, who have been there to listen to me and share encouragement and make me feel loved, thank you. Lastly, I must acknowledge my husband, Nicholas Ward. I would not be where I am without you. I am eternally grateful for my life and for all the wonderful people who make it what it is.

TABLE OF CONTENTS

Page

Page

LIST OF FIGURES

CHAPTER I

INTRODUCTION

How will Earth's climate system respond to rapidly increasing atmospheric carbon dioxide (CO_2) concentrations from anthropogenic carbon emissions? In the last 200 years, the increase in atmospheric CO_2 (~135 ppm) has surpassed the typical CO_2 change across entire glacial-interglacial cycles (~80-100 ppm) which occur on the order of thousands of years (Kohfeld et al., 2005). With the rate of modern atmospheric CO_2 increase surpassing that which occurred across several millennia, we must look to how the Earth responded in the past to carbon cycle changes to understand how the climate will respond in the future. Much uncertainty remains as to how the Earth will respond to modern accelerated atmospheric carbon input, yet a closer observation of the global carbon cycle and the intricacies of its many components and feedbacks will help shed light on possible outcomes. We look to models to improve understanding and predict global reactions to atmospheric carbon influx, however such models require calibration through reconstruction and evaluation of historic climate analogs.

Changes in ocean circulation and chemistry act as the main drivers of changes in atmospheric CO_2 across glacial-interglacial cycles (Broecker, 1982; Sigman & Boyle, 2000). Because of the large reservoir of DIC in the ocean, it is a key component of the carbon cycle and serves as a global buffer for atmospheric CO_2. Within the air-sea CO_2 exchange, equilibrium is controlled by differences in partial pressure of CO_2 (pCO_2) in the atmosphere and at the sea surface. When pCO_2 is greater in the atmosphere than the surface ocean, the ocean absorbs atmospheric CO_2 and acts as a sink. When pCO_2 is lower in the atmosphere than the ocean, the ocean releases CO_2 and it acts as a source. When the surface ocean absorbs CO_2, it undergoes a

series of reactions that buffer seawater pH. Carbon dioxide first reacts with H_2O to form carbonic acid (H_2CO_3), then loses a hydrogen ion (H^+) to form bicarbonate (HCO_3^-). Bicarbonate then loses a H^+ and becomes carbonate ion (CO_3^{2-}) (Emerson & Hedges, 2008):

$$CO_2 + H_2O \leftrightarrow H_2CO_3 \leftrightarrow HCO_3^- + H^+ \leftrightarrow CO_3^{2-} + 2H^+ \quad [1]$$

This process increases free H^+ in seawater and decreases seawater pH. Carbonate system reactions are reversible and either increase or decrease pH depending upon the ocean's absorption or release of CO_2. Seawater with low pH indicates increased presence of protons and favors proton donor H_2CO_3, while seawater with high pH indicates fewer protons and favors proton acceptors HCO_3^- and CO_3^{2-} (Fig. 1; Wolf-Gladrow et al., 2007). Because the air-sea CO_2 gradient strives for equilibrium, the global ocean increases carbonate buffering during interglacial periods when atmospheric CO_2 concentrations are high, which drives down pH and CO_3^{2-} concentrations (Sanyal et al. 1995). During glacial periods characterized by lower atmospheric CO_2 concentrations, the ocean slows carbonate buffering, which raises pH and CO_3^{2-} concentrations (Spero et al., 1997). Although the ocean is globally characterized by higher CO_2 concentrations during interglacial periods and lower CO_2 during glacial periods, changes in the air-sea carbon flux vary locally.

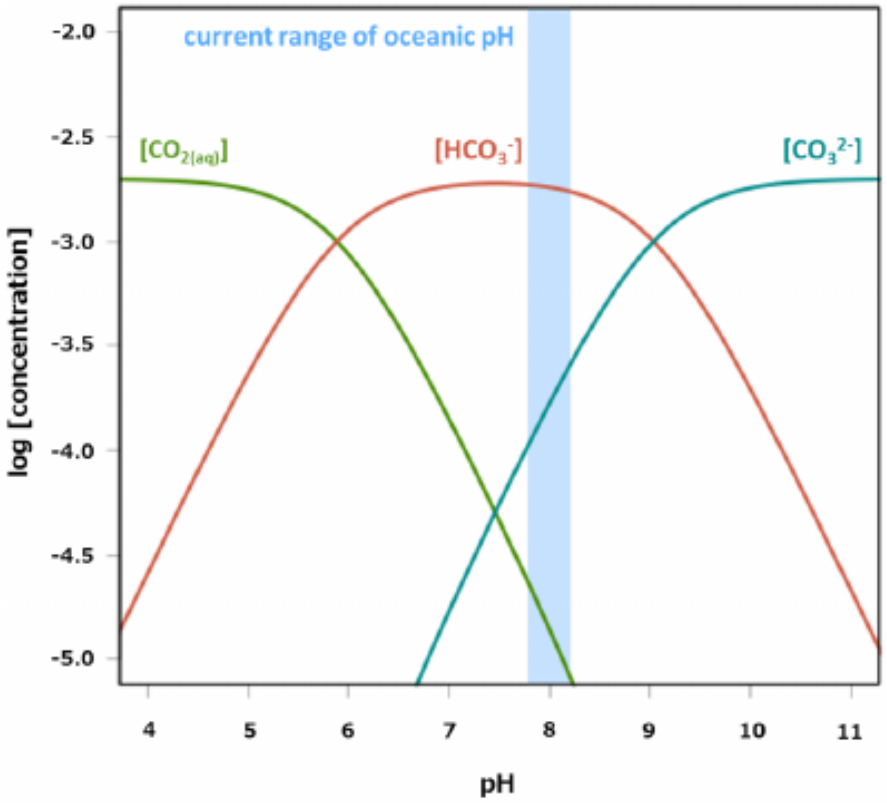

Figure 1. Bjerrum plot of carbon species abundance shift with pH. The green line indicates [CO_2], red indicates [HCO_3^{2-}], and teal indicates [CO_3^{2-}] (from Heinze et al., 2015).

Today, with elevated atmospheric CO_2 concentrations from anthropogenic emissions, the ocean acts as a net carbon sink. High atmospheric CO_2 increases the air-sea pressure gradient and causes the ocean to absorb excess carbon. A recent study estimated the ocean absorbed roughly 30% of anthropogenic CO_2 emissions between 1994 and 2007 (Gruber et al., 2019). Although a net sink, the ocean also acts as a source of atmospheric CO_2 in locations where cold, CO_2-rich water upwells (Gruber et al., 2011). Shifts in the ocean's absorption or release of CO_2 due to various biological, physical, and chemical processes influence the global carbon cycle. A better understanding of how these processes interact with the carbon cycle in key oceanographic

regions is needed to determine how the global ocean will respond to changes in atmospheric CO_2 and to improve accuracy of future climate predictions.

The eastern equatorial Pacific (EEP) plays a critical role in the global carbon budget and acts as major source of CO_2 to the atmosphere today with coastal and equatorial upwelling and the El Niño-Southern Oscillation (ENSO) causing excess CO_2 outgassing (Fielder & Talley, 2006). It has been shown, however, that small perturbations in the climate system can cause large shifts in the absorption or release of CO_2 in this region (Takahashi et al., 2002). Therefore, it is critical to understand connections between oceanic outgassing of CO_2 in the EEP and atmospheric CO_2 as atmospheric CO_2 concentrations rise rapidly over the next several decades.

PREVIOUS STUDIES

Previous studies found marked shifts in atmospheric pCO_2 across glacial-interglacial transitions, with CO_2 concentrations varying between ~180 ppm to 280 ppm over the last 800,000 years of climate changes (Barnola et al., 1987; Tripati et al., 2009). Atmospheric CO_2 oscillations were also linked with changes in global temperature, precipitation, atmospheric and oceanic circulation, and sea level (Lambeck & Chappell, 2001; Petit et al., 1999; Tripati et al., 2009). Various archives and proxies have shown that glacial periods are characterized by lower atmospheric CO_2 concentrations, higher surface water [CO_3^{2-}], decreased global temperature and precipitation rates, and lower sea levels (Foster, 2008; Hönisch & Hemming, 2005; Lambeck & Chappell, 2001; Sanyal et al., 1995; Zeebe, 2012). Conversely, interglacial periods are characterized by higher concentrations of atmospheric CO_2, lower surface water [CO_3^{2-}], higher global temperatures and rates of precipitation, and higher sea levels (Barnola et al., 1987; Schmittner & Galbraith, 2008; Sigman & Boyle, 2000).

Although there is a strong positive correlation between atmospheric CO_2 and global temperature on glacial-interglacial timescales (Petit et al.,1999), the ultimate driver of global atmospheric CO_2 fluctuations remains unclear. It is widely accepted that changes in ocean chemistry and circulation drive atmospheric CO_2 changes across glacial-interglacial transitions and many processes have been proposed to play a role (Broecker, 1982; Sigman & Boyle, 2000). Terrestrial carbon storage, ocean temperature and circulation, ocean-air carbon exchange, the marine carbon cycle, and oceanic nutrient utilization in high-latitudes all work to regulate atmospheric CO_2, but it is likely the combination of these processes that creates the global carbon feedback seen across climate cycles (Brovkin et al., 2007; Kohfeld et al, 2005; Peacock et al., 2006; Sigman & Boyle, 2000).

Current investigations also emphasize the role of variations in the biological carbon pump in glacial-interglacial CO_2 changes, which is the process of organic carbon transfer from the surface ocean to sequestration in the deep ocean through biological processes (Kohfeld et al., 2005; Sigman & Boyle, 2000). An increase in biological pump strength results in increased deep oceanic carbon storage, as biological productivity in the surface ocean draws down atmospheric CO_2. Explanations for enhancement of the biological pump during glacial periods include increases in nitrate or phosphate in surface waters, shifts in phytoplankton species abundance or community composition, and increased iron-rich dust fertilization in otherwise high-nutrient low-chlorophyll (HNLC) regions (Bopp et al., 2003; Broecker, 1982; Kohfeld et al., 2005).

The effect of iron-rich dust delivery on biological pump stimulation has gained much attention in the last few decades due to its potential to remove CO_2 from the atmosphere. Iron is often a limiting micronutrient for phytoplankton growth (Meyers, 2007). Low iron concentrations in seawater across many regions of the ocean restrict carbon fixation. These

regions are termed high nutrient low chlorophyll (HNLC) because there are high macronutrient concentrations (e.g., nitrate, phosphate, and silicate) but low phytoplankton growth due to the lack of iron in the correct stoichiometric proportions (Martin, 1994; Tyrell et al., 2005). Approximately 30% of the ocean is considered HNLC, but the Southern Ocean and EEP are the most significant HNLC regions (Martin et al., 1994; Tyrell et al., 2005; Watson et al., 2000). Although we have known about iron limitation of phytoplankton growth since the 1920's (Hart, 1934), Martin did not propose his "iron hypothesis" until 1990 (Martin, 1990). According to the "iron hypothesis", increased delivery of iron to the oceans during glacial periods stimulated the biological pump and Martin hypothesized this was the main driver of atmospheric CO_2 shifts across glacial-interglacial periods. Through experimentation in HNLC zones, particularly in the EEP, Martin found that it was possible to strengthen biological productivity using artificial inputs of iron (Martin, 1990; Martin et al. 1991, 1994). Although later studies refuted Martin's hypothesis and revealed other drivers of atmospheric CO_2 variability (Aumont & Bopp, 2006; Bopp et al., 2003; Watson et al., 2000), increased delivery of iron-rich dust during cold, glacial periods can stimulate the biological pump and increase carbon sequestration (Broecker & Henderson, 1998; Kohfeld et al., 2005; Martin, 1990).

The EEP is one of the largest HNLC locations in the global oceans and yet it supports 5-10% of global marine productivity (Loubere, 2000; Pennington et al., 2006). It is also the greatest source of oceanic CO_2 to the atmosphere, with coastal upwelling of CO_2-rich deep water outgassing over 20 Pg-$C y^{-1}$ (Takahashi et al., 2009; Loubere, 2000; Martínez-Botí et al., 2017). Despite high rates of productivity in the region today, the rate of deep-water CO_2 efflux surpasses the rate of CO_2 influx from the biological pump and results in a net source of CO_2 to

the atmosphere. Theoretically, if dust fertilization enhanced biological productivity in the region, it could overcome the efflux of upwelling CO_2 and become a net carbon sink.

Using excess ^{230}Th-derived fluxes of ^{232}Th and excess barium (xsBa), Loveley et al. (2017) reconstructed dust flux and export production, respectively, in the EEP over the last 80 kyr. They found that increased delivery of iron-rich dust to the EEP during cold Heinrich events increased biological productivity in the region. They hypothesized that this increased efficiency of the biological pump, which caused the region to absorb atmospheric CO_2, created a positive feedback for the cold, glacial state, bolstering conclusions drawn by Martínez-Botí et al. (2015). Using boron isotopes as a proxy for pH, Martínez-Botí et al. (2015) determined that the EEP switched from a source to a sink of CO_2 over the last deglaciation. They theorized that increased dust flux and iron fertilization stimulated the biological pump and caused a shift in CO_2 flux in the region. This could occur, for instance, if the Intertropical Convergence Zone (ITCZ) shifted southward and enabled northeast trade winds to carry iron-rich dust from the Sahara to surface waters in the EEP. If this happened in the past, fluctuations in the strength of the biological pump may have caused the EEP to become a CO_2 sink and significantly altered the carbon cycle.

In comparison, Spero (unpublished data) observed a prominent shift in the EEP carbon cycle during the MIS 5a-4 transition (96 to 60 kyr), across the last glaciation at the start of the last glacial period. He used δ^{13}C in the planktic foraminifera *Globigerinoides ruber* (*G. ruber*) and *Trilobatus sacculifer* (*T. sacculifer*) as a proxy for $\Delta[CO_3^{2-}]$ in core TR163-19 (2°15.5′N, 90°57.1′W, 2348 m water depth) located on the Cocos Ridge and found evidence of a carbon system shift in the EEP from 96 to 60 kyr. Spero noted rapidly increased surface water $[CO_3^{2-}]$ across the transition, which indicated a change in the carbon cycle in the region. The scope and cause of the shift, however, remains unknown.

Because of the known connection between atmospheric CO_2 and surface water [CO_3^{2-}], a record of past changes in surface water [CO_3^{2-}] in the EEP would help determine a possible link between dust-driven iron fertilization and carbon cycling in the region. Furthermore, a surface water [CO_3^{2-}] record would shed light on the magnitude and driver of changes in the air-sea CO_2 exchange in the EEP across climate transitions.

RESEARCH QUESTION AND HYPOTHESIS

Questions remain as to the primary driver of global atmospheric CO_2 variability across glacial-interglacial cycles and further investigation into CO_2 changes in key oceanographic regions is needed. As the largest oceanic source of CO_2 to the atmosphere today, the EEP is a vital component of the global carbon cycle, but changes in CO_2 outgassing in the past hold implications for the future. Did the EEP switch to a CO_2 sink over the last deglaciation (25 kyr to present) and last glaciation (MIS 5a-4, 96 to 60 kyr)? If so, what caused the changes and what role do these changes play in regulation of global atmospheric CO_2?

Here, I test hypotheses set forth by Martínez-Botí et al. (2015) and Loveley et al. (2017). I seek to determine if increased delivery of iron-rich dust to the EEP stimulated biological productivity and caused the region to become a CO_2 sink across cold climate events. Moreover, I test the hypothesis formulated by Spero (unpublished) that surface waters in the EEP experienced a significant increase in [CO_3^{2-}] as the background climate state transitioned into the last ice age (96 to 60 kyr).

In order to address these questions, I reconstruct changes in surface water [CO_3^{2-}], an indicator of changes in the carbonate chemistry in the EEP over the last deglaciation (25 kyr to present) and glaciation (96 to 60 kyr) using a multi-proxy approach. I use B/Ca ratios in the near-surface dwelling planktic foraminifera *Globigerina bulloides* (*G. bulloides*) and $\delta^{13}C$ differences

in the surface-dwelling planktic foraminifera *G. ruber* and *T. sacculifer* as proxies for surface water [CO_3^{2-}] in the high-resolution core MV1014-17JC (00º10.83'S, 85º52.00'W; 2846 m water depth) recovered from the Carnegie Ridge (Fig. 2). Because surface water [CO_3^{2-}] is influenced by oceanic pCO_2, I reconstruct surface water [CO_3^{2-}] changes in the EEP to investigate changes in CO_2 uptake or outgassing in the region across glacial climate transitions. Furthermore, I explore potential drivers of these changes and implications for regional and global climate evolution.

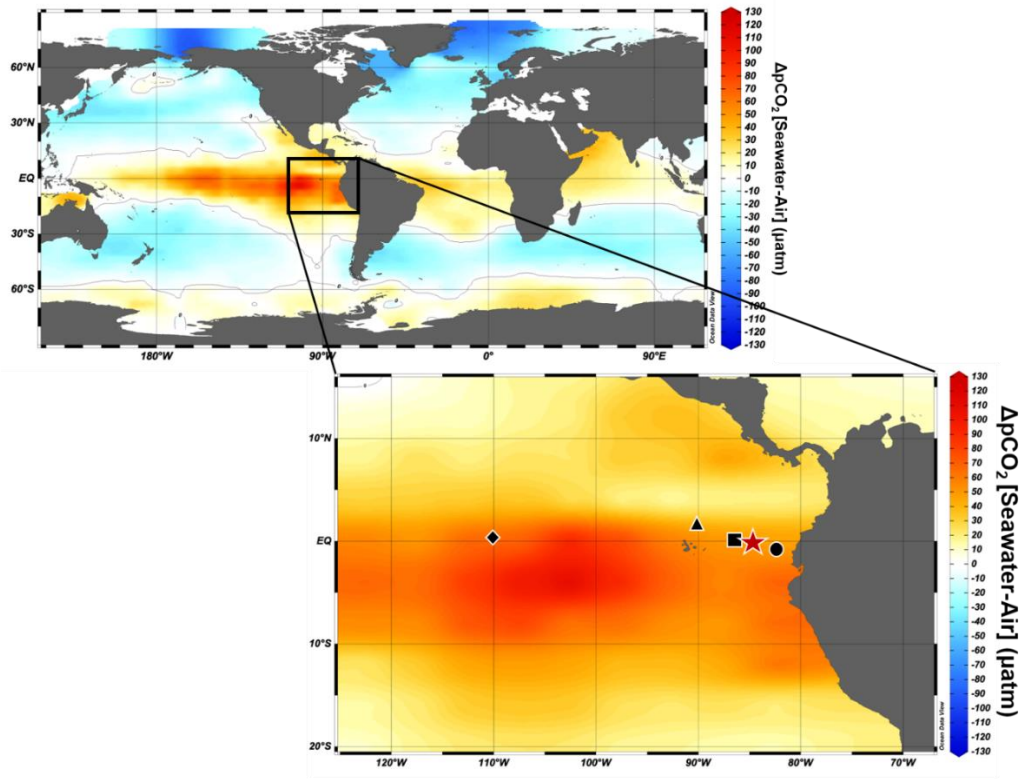

Figure 2. Study location in the EEP and ΔpCO_2 [seawater-air](µatm). This study and Loveley et al. (2017) use core MV1014-17JC (red star), Martínez-Botí et al. (2015) use core ODP1238 (black circle), and Spero (unpublished) use core TR163-19 (black triangle). Also pictured is core ME0005A-24JC (Dubois et al., 2011) (black square) and core ODP849 (Hoogakker et al., 2018) (black diamond). Generated in Ocean Data View using ΔpCO_2 [seawater-air] data from Takahashi et al. (2009).

CHAPTER II

METHODOLOGY

AGE MODEL

A preliminary age model for core MV1014-17JC was developed by Loveley et al. (2017) using a combination of ten radiocarbon dates on the planktic foraminifera *Neogloboquadrina dutertrei*, $\delta^{18}O$ tie points at MIS boundaries, and the presence of the Los Chocoyos ash layer dated at 84 kyr. Assuming constant sedimentation rates between radiocarbon dates and tie points, ages were linearly interpolated between points. Peaks in dust flux coinciding with Heinrich events enabled further tuning of the age model to the timing of Heinrich events in the absolute U/Th dated Hulu cave speleothem records.

B/CA PROXY

I used B/Ca ratios in the planktic foraminifera *G. bulloides* to reconstruct $[CO_3^{2-}]$ using a species-specific calibration developed by Krupinski et al. (2017). Krupinski et al. (2017) found a correlation between B/Ca in *G. bulloides* and surface ocean $[CO_3^{2-}]$ (µmol/kg) in 37 modern cattercore tops across the Pacific Ocean:

$$B/Ca_{\textit{G. bulloides}} = [CO_3^{2-}] * 0.319(\pm 0.031) - 12.69(\pm 5.29). \quad [2]$$

They found a positive relationship between B/Ca and $[CO_3^{2-}]$ controlled by calcification rates causing greater boron uptake during faster rates of calcification. Carbonate ion concentrations control calcite saturation state ($\Omega_{calcite}$) in seawater with greater concentrations of CO_3^{2-} increasing $\Omega_{calcite}$. Increased $\Omega_{calcite}$ increases calcification rates in seawater, which in turn increases B/Ca ratios in foraminiferal tests as rapid calcification results in uptake of molecules other than calcite (e.g., B) (Krupinski et al., 2017).

I measured B/Ca ratios in *G. bulloides* samples from the last deglaciation and glaciation using methods outlined in Schmidt et al. (2012), modified for boron-free cleaning and B/Ca measurements. Depending on availability, I picked roughly 120 *G. bulloides* from 25 intervals (~3,000 individuals) in core MV1014-17JC spanning the last deglaciation (25 kyr to present) and from 75 intervals (~9,000 individuals) spanning across the last glaciation (96 to 60 kyr). For each interval, I crushed, homogenized, and divided the foraminiferal tests into two equal aliquots to allow for duplicate analyses when sample size permitted. I then sonicated and rinsed each sample with boron-free ultrapure water and methanol to remove clays and subjected them to hot water baths with an oxidative solution to remove organic matter and a reductive solution to remove metal oxides. I transferred the samples to boron-free acid-leached vials, leached them with diluted nitric acid, and did a final rinse with boron-free ultrapure water.

Prior to analysis, samples were dissolved with boron free 2% HNO_3. I analyzed the samples on an Element XR inductively coupled plasma mass spectrometer (ICP-MS) in the COSMIC facility at ODU for a suite of minor and trace elements including B, Ca, Mg, Al, Fe, and Mn. I used linear calibrations to determine sample element/Ca ratios based on calibration standards measured multiple times during each analysis and made corrections based on blanks analyzed throughout each analysis run. Al/Ca, Fe/Ca, and Mn/Ca ratios were monitored as indicators of thoroughness of the cleaning process. High Al/Ca indicates the presence of Al-silicates within detrital clays, and elevated Fe/Ca and Mn/Ca indicate the presence of metal oxides not eliminated during cleaning. Analyses with Al/Ca and Fe/Ca > 200 mmol/mol were discarded, but samples with high Mn/Ca (> 200 mmol/mol) was not excluded because high Mn/Ca is common in foraminiferal tests from the Panama Basin due to hydrothermal activity in the region (Boyle, 1983; Pena et al., 2005, 2008; Umling et al., 2018). Because samples with

high Mn/Ca were included in our analysis, we confirmed weak covariance between Mn/Ca and B/Ca using linear regression (R^2 = 0.27, n=117). A total of 152 analyses (including replicates) were done across both glacial transitions. Twenty-one samples were discarded due to high Al/Ca and Fe/Ca (> 200 mmol/mol) which indicated contamination, one discarded due to insufficient sample size resulting in a negative (invalid) B/Ca count, and thirteen were discarded due to high blank measurements indicating instrumentation error. Therefore, 117 samples were considered valid for my reconstructions. I ran a set of matrix-matched consistency standards with known B/Ca ratios of 34.2, 44.5, and 55.9 µmol/mol recurrently during each ICP-MS run to calculate analytical precision of the measurements. However, I ended up excluding the 55.9 µmol/mol standard due to the fact that my samples had lower B/Ca ratios. I then calculated [CO_3^{2-}] from measured B/Ca ratios using Eq. 2. Analytical error from standards, duplicate analysis standard deviations, and calibration error were combined to produce total error.

ALTERNATIVE *G. BULLOIDES* MORPHOTYPE

Presence of a genetically distinct morphospecies of *G. bulloides* complicates the B/Ca proxy. A highly calcified morphotype of *G. bulloides*, termed encrusted *G. bulloides*, is shown to record lower temperatures and thought to calcify in colder waters, producing offset $\delta^{18}O$ values and Mg/Ca ratios compared to its unencrusted, "normal" counterpart (Bemis et al., 2002; Hendy & Kennett, 2000; Sauter & Thunell, 1991). Encrusted *G. bulloides* have been found in the Pacific Ocean in waters off Southern California, New Zealand, and Chile. Its presence in samples used for paleoceanographic reconstructions can skew results (Osborne et al. 2016; Krupinski et al., 2017). Krupinski et al. (2017) observed similarity in B/Ca and Mg/Ca ratios between encrusted and normal *G. bulloides* in their samples, however published a calibration for samples including both morphotypes and one for those with only normal *G. bulloides*.

To determine the appropriate calibration for *G. bulloides* at 17JC, I performed an area density analysis outlined in Osborne et al. (2016). Forty individuals visually undamaged and free from metal oxide or clay coatings were randomly chosen from six intervals across notable climate events across the deglaciation: 3.5 kyr (late Holocene), 7.9 kyr (early Holocene), 12.1 kyr (Younger-Dryas), 13.6 kyr (Bølling-Allerød), 15.5 (Heinrich Stadial 1), and 21.2 kyr (Last Glacial Maximum). These individuals were photographed through a microscope and digitally analyzed on the image processing software ImageJ (Schneider et al., 2012) to measure projected surface area and Feret diameter and individually weighed on an ultra-microbalance. Area density (weight/projected area) and size-normalized shell weights (weight/Feret diameter) were computed and plotted against each other. A linear model was fit to the data (Fig. 3) and the regression (R^2=0.916, m=4.1E-3, b=4.0E-6) was compared to the two regression lines in Osborne et al. (2016) representing encrusted *G. bulloides* (R^2=0.36, m=1.44E-3, b=6.75E-5) and normal, unencrusted *G. bulloides* (R^2=0.29, m=1.65E-3, b=4.21E-5). While our regression line does not match either the unencrusted or encrusted regression lines set forth in Osborne et al. (2016), it lies below the encrusted *G. bulloides* regression line. Furthermore, Osborne et al. (2016) found a right-skewing distribution of area densities within encrusted *G. bulloides* leaning toward greater area density. Distribution of area densities from 17JC (Fig. 4) is centered around 6.0E-5 $\mu g/\mu m^2$, similar to the unencrusted distribution found in Osborne et al. (2016). This evidence indicates an absence of encrusted *G. bulloides* in 17JC. I therefore chose to use the unencrusted B/Ca: $[CO_3^{2-}]$ calibration in Krupinski et al. (2017) for my downcore records.

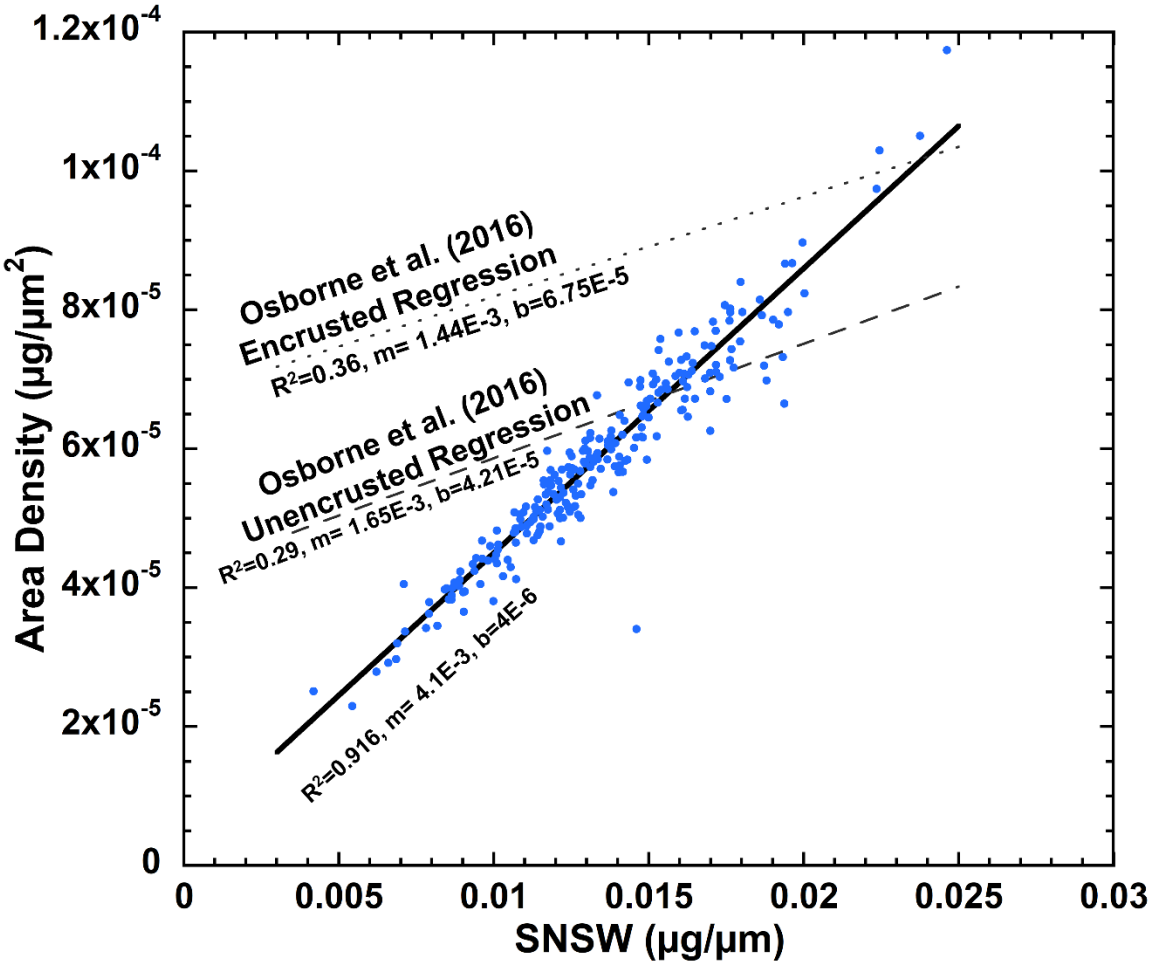

Figure 3. Area density (µg/µm^2) and size-normalized shell weights (µg/µm). Blue dots represent individuals from six intervals across the deglaciation in 17JC. A linear regression was performed and is represented by the black line. Regression lines for unencrusted *G. bulloides* (dashed line) and encrusted *G. bulloides* (dotted line) from Osborne et al. (2016) are also shown.

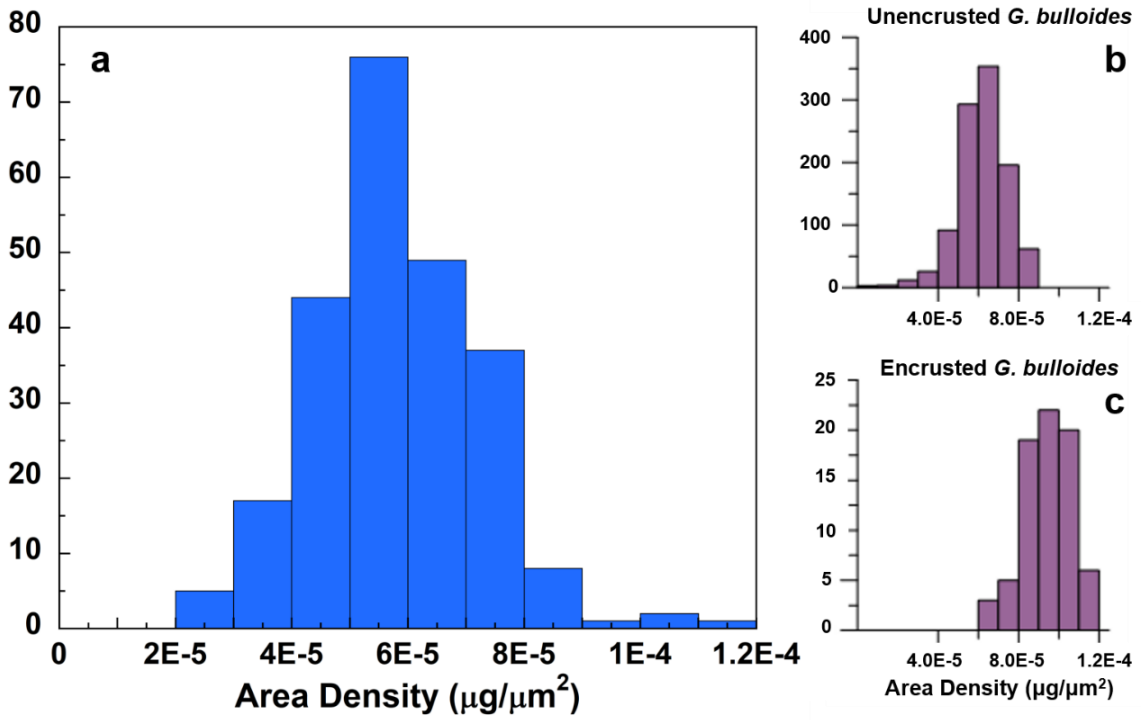

Figure 4. Area density (μg/μm^2) histograms. a) Area density histogram for 17JC samples. b) Osborne et al. (2016) histogram for unencrusted *G. bulloides*. c) Osborne et al. (2016) histogram for encrusted *G. bulloides*.

δ^{13}C PROXY

Carbonate ion concentrations were reconstructed using the $\delta^{13}C$ to $\Delta[CO_3^{2-}]$ proxy in the planktic, upper mixed layer-dwelling foraminifera species *G. ruber* and *T. sacculifer*. Spero et al. (1997) first observed a relationship between the $\delta^{13}C$ of planktic foraminifera and seawater carbonate chemistry and found that the $\delta^{13}C$ value in planktic foraminifera is controlled by the ratios of dissolved inorganic carbon in seawater, as well as by respiration and symbiont photosynthesis. More specifically, they found that planktic foraminiferal $\delta^{13}C$ decreases with increasing surface water $[CO_3^{2-}]$. They experimentally derived species-specific slopes for the $\delta^{13}C$: $[CO_3^{2-}]$ relationship for *G. ruber* and *T. sacculifer* and noticed that the species have

different sensitivities to changes in surface water [CO_3^{2-}]. Therefore, assuming dissolution and bioturbation would act on both species equally, the difference in $\delta^{13}C$ between *G. ruber* and *T. sacculifer* can be used a proxy for changes in surface water [CO_3^{2-}] (Spero et al., 1999).

Following methods outlined in Spero et al. (1999), I picked 20 *G. ruber* and 4 to 30 *T. sacculifer* shells, depending on availability, from 39 intervals from core MV1014-17JC spanning the last deglaciation and 75 intervals spanning the last glaciation totaling ~2,200 and ~3,400 individuals, respectively. I used multiple shells from each interval to average the impacts of vital effects (respiration and symbiont photosynthesis) on shell $\delta^{13}C$ and to ensure any changes in shell $\delta^{13}C$ solely reflected mean seawater $\delta^{13}C$ influence (Spero et al., 1999). Samples were placed into glass vials in sets of 10 to avoid breakage and cleaned for stable isotope analysis. I filled each vial ~2/3 full with methanol and sonicated each for 1-3 seconds to loosen clays and organic material from the shells. Using a pipette, I removed the tests from each vial, dried, weighed, and placed them into new vials. Each vial was sealed, wrapped individually, and logged. I sent the samples to our collaborator, Dr. Howard Spero, at the University of California Davis for stable isotope analysis ($\delta^{13}C/\delta^{14}C$ and $\delta^{16}O/\delta^{18}O$) on a Micromass Optima isotope ratio mass spectrometer (IRMS).

Based on measured $\delta^{13}C$ data for both species, [CO_3^{2-}] was calculated at any time interval, *t*, using equations defined in Spero et al. (1999):

$$(\delta^{13}C_{sacc})_t = \delta^{13}C_{\Sigma CO2} + m_{sacc} * [CO_3^{2-}]_t \quad [3]$$

and

$$(\delta^{13}C_{ruber})_t = \delta^{13}C_{\Sigma CO2} + m_{ruber} * [CO_3^{2-}]_t \quad [4]$$

with m_{sacc} = -0.0047 ‰µmol^{-1}kg^{-1} as the experimentally derived slope of the *T. sacculifer* $\delta^{13}C$ and m_{ruber} = -0.0089 ‰µmol^{-1}kg^{-1} as the experimentally derived slope of the *G. ruber* $\delta^{13}C$.

Changes in downcore $[CO_3^{2-}]$, defined as the difference between any interval, *t*, and the core top, *ct*, were calculated:

$$\Delta[CO_3^{2-}]_{t\text{-}ct} = (\delta^{13}C_{sacc} - \delta^{13}C_{ruber})_{t\text{-}ct} / (m_{sacc} - m_{ruber}) \quad [5]$$

where $m_{sacc} - m_{ruber} = 0.0042$ $\mu mol^{-1}kg^{-1}$. Spero et al. (1999) notes calibration error for this proxy is $\pm$ 40 µmol/kg. The $\delta^{13}C$-derived $\Delta[CO_3^{2-}]$ record was then smoothed with a 3-point running mean.

B/CA-DERIVED $[CO_3^{2-}]$ RECONSTRUCTION

As the B/Ca proxy calculates $[CO_3^{2-}]$ and the $\delta^{13}C$ proxy calculates $\Delta[CO_3^{2-}]$, or the change in $[CO_3^{2-}]$ downcore, I normalized the B/Ca derived record to the core top B/Ca calculated $[CO_3^{2-}]$ to derive $\Delta[CO_3^{2-}]$. I then compared the two $\Delta[CO_3^{2-}]$ records against the modern surface water $[CO_3^{2-}]$ of 200 µmol/kg (Tyrell & Zeebe, 2004). Also, because temporal changes in atmospheric pCO_2 alter global surface water $[CO_3^{2-}]$ on centennial and longer time scales, it is necessary to consider this influence on the calculated B/Ca-derived $[CO_3^{2-}]$ record in the past. During the last glacial period, atmospheric pCO_2 was lower, resulting in an increased in global surface water $[CO_3^{2-}]$. Raven et al. (2005) quantified the influence of atmospheric pCO_2 on seawater pH and determined that a 100-ppm increase in atmospheric pCO_2 decreases seawater pH by 0.145 units. This translates to about a 46-µmol/kg decrease in $[CO_3^{2-}]$ (Feeley et al., 2009). Using this relationship, I interpolated pCO_2 data from Dome C and the Vostok ice core record (Monnin et al., 2001; Petit et al., 1999; Pépin et al., 2001; Raynaud et al., 2005) and calculated predicted change in surface water $[CO_3^{2-}]$ due only to atmospheric pCO_2 across both glacial transitions. I then subtracted the predicted $[CO_3^{2-}]$ change due to a lowering of atmospheric pCO_2 to the B/Ca-derived $[CO_3^{2-}]$ to account for the influence of temporal changes in atmospheric pCO_2.

CHAPTER III

RESULTS

B/CA

Boron to calcium ratios range from 16.2 to 54.9 µmol/mol with an average of 37.7 µmol/mol (n=85). The average analytical error determined from instrument precision is 0.54 µmol/mol (1.42%). Sample abundance permitted replicate analysis of 31 samples (27%) of samples and replicate relative standard deviation (RSD) range from 0.10 µmol/mol (1.32%) to 2.9 µmol/mol (7.7%), with an average replicate RSD of 1.55 µmol/mol (4.12%). Combined replicate and analytical RSD ($\sqrt{RSD_A^2 + RSD_B^2}$) yield an error of $\pm$ 1.64 µmol/mol (4.36%).

DEGLACIATION

As shown in Fig. 5a, B/Ca values across the deglaciation range from 29.6 to 55.0 µmol/mol, with an average of 41.9 µmol/mol and a standard deviation of 6.17 µmol/mol. The average B/Ca is 34.5 µmol/mol (n=5) in the glacial portion of the record (25 to 20 kyr), 42.3 µmol/mol (n=11) in the deglacial portion (20 to 11.5 kyr), and 46.0 µmol/mol (n=8) in the interglacial portion, or the Holocene, (11.7 kyr to present).

At the beginning of the record at 25.1 kyr, B/Ca ratios increase slightly until 24.2 kyr, then decrease until the mid-Last Glacial Maximum (LGM) where (at 21.2 kyr) values reach 29.6 µmol/mol, the lowest across the deglaciation. After 21.2 kyr, ratios increase until 16.9 kyr, just before Heinrich Stadial 1 (H1), where they then decrease to 35.8 µmol/mol. Across H1 into the Bølling-Allerød (BA) and through the Younger-Dryas (YD), ratios of B/Ca remain fairly stable. Following the YD, into the early Holocene (EH), B/Ca decreases to the second lowest value of 34.4 µmol/mol at 9.4 kyr, then increases across the mid to late Holocene.

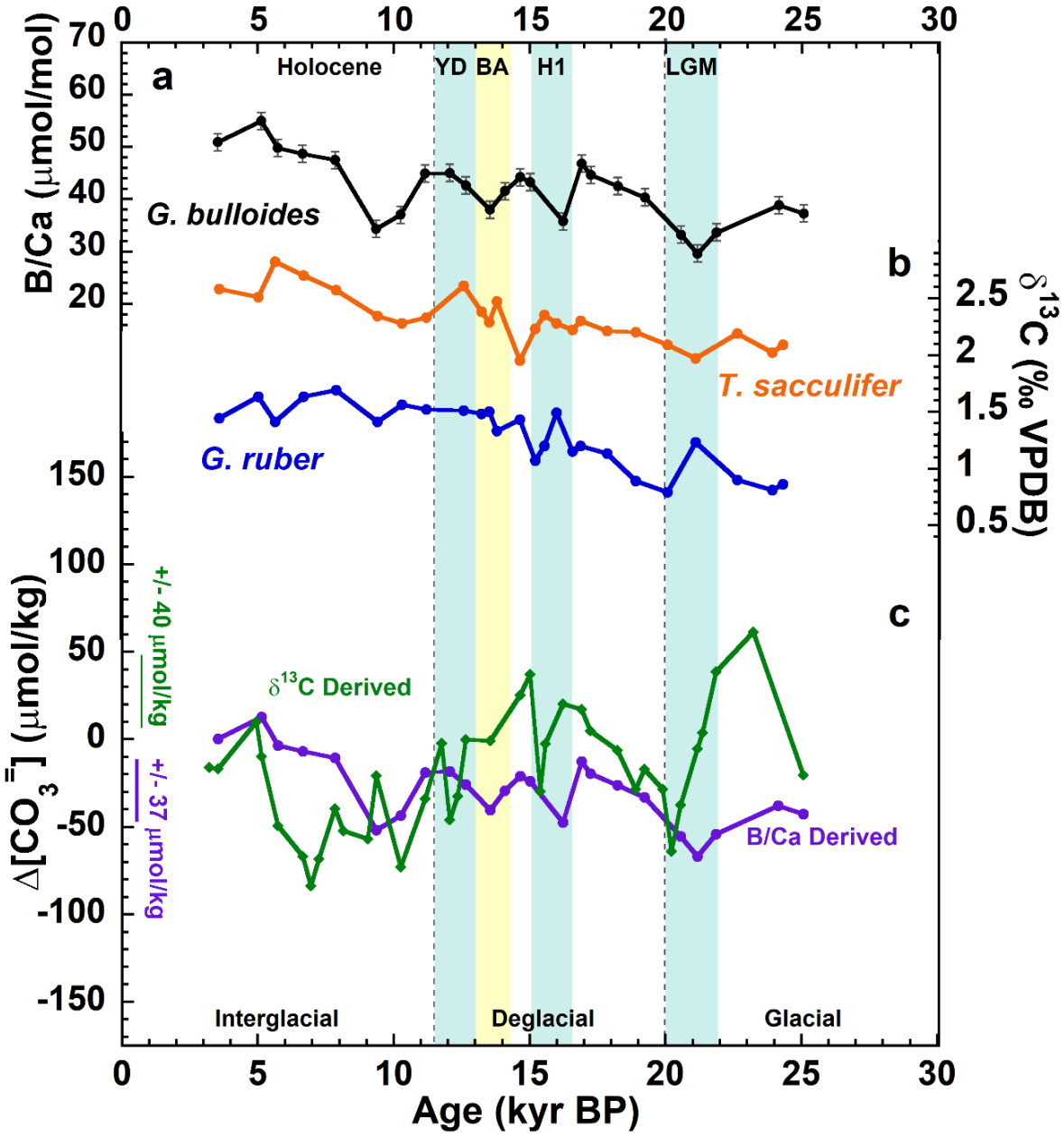

Figure 5. Proxy reconstruction from 25 kyr to present. a) Measured B/Ca (µmol/mol) in *G. bulloides*. Error bars represent ±1.64 µmol/mol (combined error). b) $\delta^{13}C$ (‰VPDB) of *T. sacculifer* is indicated in orange and *G. ruber* indicated in blue. Analytical error bars of ± 0.03‰VPDB are too small to be seen. c) $\Delta[CO_3^{2-}]$ (µmol/kg) calculated from $\delta^{13}C$ in *T. sacculifer* and *G. ruber* is indicated in green with an error of ± 40 µmol/kg and $\Delta[CO_3^{2-}]$ calculated from B/Ca from *G. bulloides* in purple with an error of ± 37 µmol/kg. The gray dashed lines represent boundaries between glacial, deglacial, and interglacial climates.

GLACIATION

Shown in Fig. 6a, B/Ca values across the glacial transition range from 16.2 to 49.8 µmol/mol, with an average of 33.5 µmol/mol and a standard deviation of 6.10 µmol/mol. Average B/Ca in the interglacial (before 72 kyr) portion of the glaciation is 33.9 µmol/mol (n=50) and average B/Ca in the glacial (after 72 kyr) portion is 31.9 µmol/mol (n=11).

The earliest part of the two records begins at 95.8 kyr in mid to late MIS5c during an interglacial period. Here, B/Ca ratios increase slightly until 94.0 kyr where values decrease from 34.1 to 16.2 µmol/mol at 92.8 kyr, the lowest value in the B/Ca glaciation record. Ratios then increase across MIS5b and remain relatively stable until mid MIS5a at 83.1 kyr where they drop from 39.7 to 16.3 µmol/mol at 77.6 kyr. Values then rapidly increase to 49.8 µmol/mol at 76.9 kyr, the highest ratio in the record. After this point, ratios decrease, then increase again to 48.0 µmol/mol at 74.1 kyr, where they then decrease slightly. From this point in late MIS5a at 73.7 kyr to mid MIS4 at 65 kyr, values remain generally constant around 32.6 µmol/mol.

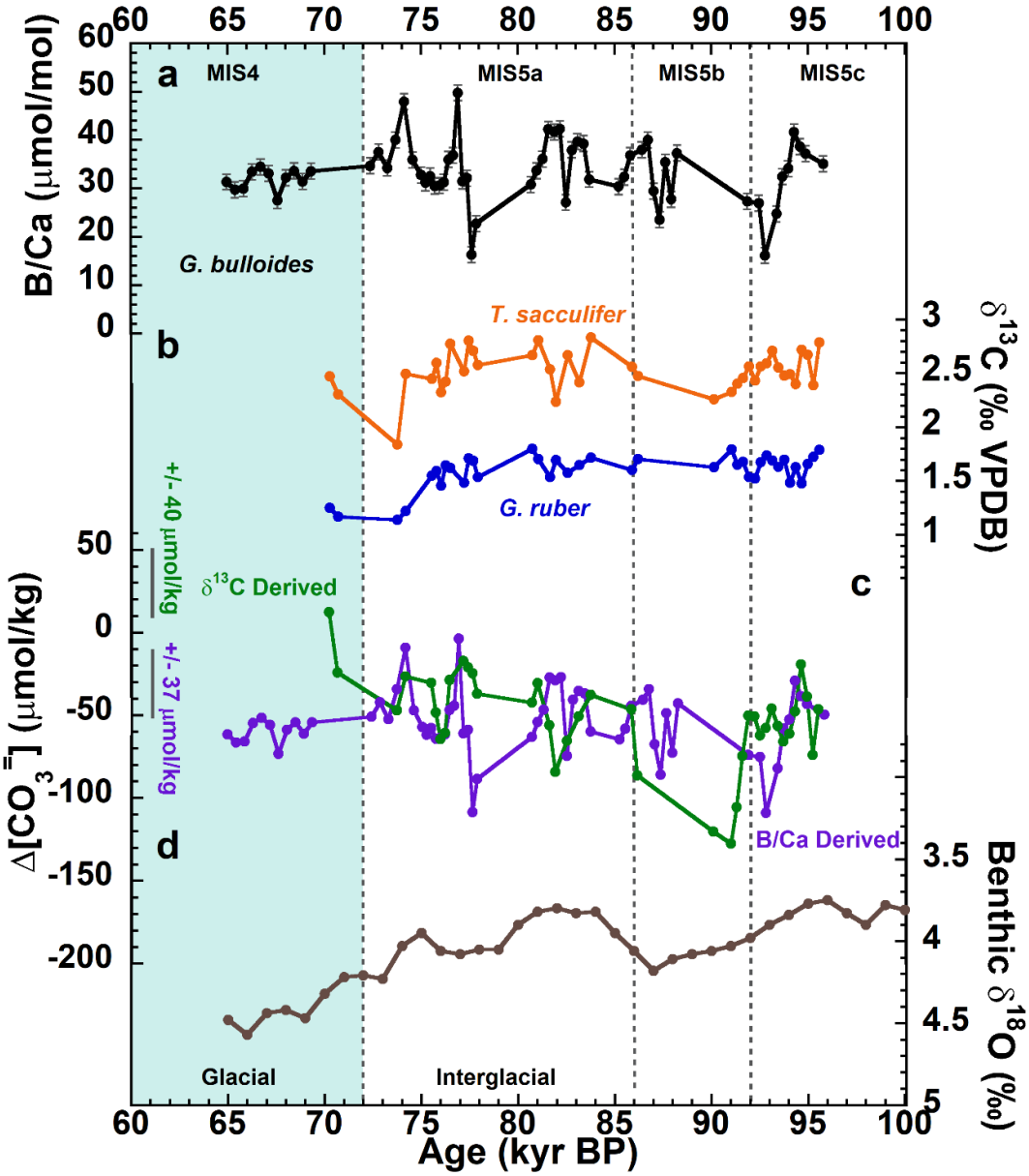

Figure 6. Proxy reconstruction across 96 to 60 kyr. a) Measured B/Ca (µmol/kg) in *G. bulloides*. Error bars represent ±1.64 µmol/mol (combined error). b) $\delta^{13}C$ (‰VPDB) of *T. sacculifer* are represented in orange and *G. ruber* by blue. Analytical error bars of ± 0.03‰VPDB are too small to be seen. c) $\Delta[CO_3^{2-}]$ (µmol/kg) calculated from $\delta^{13}C$ in *T. sacculifer* and *G. ruber* are in green with an error of ± 40 µmol/kg and $\Delta[CO_3^{2-}]$ calculated from B/Ca from *G. bulloides* in purple with an error of ± 37 µmol/kg. d) Benthic $\delta^{18}O$ from Lisiecki & Raymo (2004) to distinguish Marine Isotope stages. The gray dashed lines represent boundaries between Marine Isotope Stages.

$\delta^{13}C$

Stable carbon isotope values range from 0.79 to 1.80‰ in *G. ruber* with an average value of 1.41‰ and a standard deviation of 0.28‰ (n=76). Stable carbon isotope values range from 1.84 to 2.83‰ in *T. sacculifer*, with an average value of 2.40‰ and a standard deviation of 0.24‰ (n=76). Analytical error on these measurements is 0.03‰ (1.56%).

DEGLACIATION

Across the deglaciation, *G. ruber* $\delta^{13}C$ values range from 0.79 to 1.69‰ (n=37), while those for *T. sacculifer* range from 1.9 to 2.82‰ (n=37)(Fig. 5b). There is a slight positive trend in $\delta^{13}C$ from glacial to interglacial climate states in the records of both species, with lower $\delta^{13}C$ values in the glacial and higher values in the interglacial. The average $\delta^{13}C$ value for *G. ruber* is 1.10‰ (n=7) in the glacial portion of the record, 1.05‰ (n=16) in the deglacial portion, and 1.45‰ (n=14) in the Holocene. Average $\delta^{13}C$ for *T. sacculifer* is 2.18‰ (n=7) in the glacial portion, 2.15‰ (n=16) in the deglacial, and 2.43‰ (n=14) in the Holocene.

Despite a 1.0‰ difference in average $\delta^{13}C$ values between foraminiferal species, because *G. ruber* and *T. sacculifer* record $\delta^{13}C_{sw}$ ($\delta^{13}C$ of dissolved inorganic carbon (DIC) in seawater) equally, changes in $\delta^{13}C$ in both records follow similar patterns just with an offset in values (see Methodology: $\delta^{13}C$ Proxy). Beginning at 25 kyr, $\delta^{13}C_{rub}$ ($\delta^{13}C$ for *G. ruber*) increases into the LGM until 21 kyr, while $\delta^{13}C_{sac}$ **(**$\delta^{13}C$ for *T. sacculifer*) increases until just before the LGM at 23 kyr. The records then show a decrease in the LGM and a subsequent increase from the late LGM into H1 at 15.5 kyr. Here, both records decrease slightly until late H1, where they then increase until the mid BA at 13.5 kyr. Both records then level off, but $\delta^{13}C_{sac}$ shows a slightly more pronounced increase than $\delta^{13}C_{rub}$ from late BA at 13 kyr into the late Holocene at 3.2 kyr.

GLACIATION

Across the glaciation (Fig. 6b), $\delta^{13}C$ values for *G. ruber* range from 1.14 to 1.80‰ (n=39), while *T. sacculifer* $\delta^{13}C$ values range from 1.84 to 2.83 ‰ (n=39). There is little difference in $\delta^{13}C$ values in the two species between interglacial and glacial climates. Average $\delta^{13}C_{rub}$ and $\delta^{13}C_{sac}$ in the interglacial period are 1.21‰ (n=2) and 2.40‰ (n=2), respectively. Across the glacial period, the average $\delta^{13}C_{rub}$ is 1.61‰ (n=37) and average $\delta^{13}C_{sac}$ is 2.53‰ (n=37). This represents an interglacial-glacial increase of 25% for *G. ruber* and a 5.5% increase for *T. sacculifer*. It should be noted, however, that although there is a 25% increase in $\delta^{13}C_{rub}$ record, the sample size in the glacial period for both species is too low to draw any definitive conclusions.

From 95.5 kyr in MIS5c to 86 kyr in early MIS5a, both $\delta^{13}C$ records remain stable around 1.65‰ for *G. ruber* and 2.52‰VPDB for *T. sacculifer*. At 86 kyr, $\delta^{13}C_{sac}$ increases slightly, while $\delta^{13}C_{rub}$ stays steady until around 75.5 kyr. At about 75 kyr, however, both $\delta^{13}C$ values decrease and reach their lowest values in the glaciation at 73.7 kyr with $\delta^{13}C_{rub}$ of 1.14‰ and $\delta^{13}C_{sac}$ of 1.84‰. The transition into the glacial period in the early part of MIS4 is marked by a slight increase in $\delta^{13}C_{rub}$ and a larger increase in $\delta^{13}C_{sac}$.

RECONSTRUCTED $\Delta[CO_3^{2-}]$ RECORDS

DEGLACIATION

B/CA DERIVED $\Delta[CO_3^{2-}]$

Across the deglaciation, B/Ca-derived $\Delta[CO_3^{2-}]$ ranges from -66.9 to 12.8 µmol/kg, with an average of -28.3 µmol/kg and a standard deviation of 19.3 µmol/kg (Fig. 5c). Average $\Delta[CO_3^{2-}]$ derived from B/Ca is -51.5 µmol/kg (n=5) in the glacial portion, -27.2 µmol/kg (n=11) in the deglacial, and -17.6 µmol/kg (n=7) in the Holocene. Boron to calcium-derived $\Delta[CO_3^{2-}]$

decreases from -37.9 µmol/kg at the start of the record at 25 kyr to -66.9 µmol/kg in the mid-LGM at 21 kyr. Values then increase 54.2 µmol/kg to -12.7 µmol/kg near the onset of H1 at 16.8 kyr. Across H1, BA, YD, and the EH, $\Delta[CO_3^{2-}]$ values remain relatively stable within $\pm$ 12.7 µmol/kg, well within error. In the EH after 9.36 kyr, $\Delta[CO_3^{2-}]$ increases to 12.7 µmol/kg, the highest point in the record. Overall, the record indicates that across the deglaciation, surface water $[CO_3^{2-}]$ remained below modern concentrations, apart from an increase in the mid-Holocene at 5.14 kyr. However, the increase above modern is still within error bounds.

$\delta^{13}C$ DERIVED $\Delta[CO_3^{2-}]$

Across the deglaciation, surface water $[CO_3^{2-}]$ variability derived from $\delta^{13}C$ ranged from -83.9 to 61.3 µmol/kg, with an average of -18.7 µmol/kg and a standard deviation of 33.3 µmol/kg (Fig. 6c). Average $\delta^{13}C$-derived $\Delta[CO_3^{2-}]$ is -3.41 µmol/kg (n=7) in the glacial portion, -5.68 µmol/kg (n=16) in the deglacial, and -41.3 µmol/kg (n=14) in the Holocene. The highest $\Delta[CO_3^{2-}]$ in the record occurs in the glacial period at 23.4 kyr, just before the LGM, at 61.3 µmol/kg. Values after this point decrease by 102 µmol/kg across the LGM in a span of 1.60 kyr and subsequently increase in the late LGM at 20.2 kyr. From the late LGM into H1, $\Delta[CO_3^{2-}]$ increases, then decreases in mid to late H1, increases in late H1, and drops across the BA. Although the record itself exhibits variability across H1, BA, and YD, values remain within error from about 20 kyr to the EH at 10.3 kyr. Carbonate ion concentrations show greater than modern values in the glacial portion of the record and near modern values from the onset of the interglacial portion at ~20 kyr until 10 kyr. From 10.3 to 5.1 kyr, values remain lower than modern until they increase to near modern concentrations at present. The $\delta^{13}C$ record suggests lower than modern values across most of the deglaciation, apart from increases above modern in the glacial and early deglacial portion of the record outside of error.

GLACIATION

B/CA DERIVED $\Delta[CO_3^{2-}]$

Across the glaciation, B/Ca-derived $\Delta[CO_3^{2-}]$ ranges from -109 to -3.66 µmol/kg, with an average of -54.6 µmol/kg and a standard deviation of 19.1 µmol/kg (Fig. 6c). There is no noticeable difference in values between glacial (n=11) and interglacial (n=50) climate, with averages of -59.8 µmol/kg and -53.5 µmol/kg, respectively. Surface water $\Delta[CO_3^{2-}]$ derived from B/Ca ratios remain within error across the majority the glaciation. The record begins in late MIS5c, where values decrease from -29.1 µmol/kg at 94.3 kyr to -109 µmol/kg at 92.8 kyr. From 92.8 kyr to 80.7 kyr, through MIS5b to late MIS5a, concentrations steady around -54.6 µmol/kg. At 80.7 kyr, values decrease again to -109 µmol/kg at 77.6 kyr, then increase to -9.25 µmol/kg at 74.1 kyr. From that point, B/Ca-derived $\Delta[CO_3^{2-}]$ stabilizes around -52.9 µmol/kg moving into the glacial climate in MIS4 until the end of the record at 64.9 kyr. In this record, $\Delta[CO_3^{2-}]$ values remain within error apart from five data points across MIS5c and 5a where the records lie outside of error. Overall, B/Ca-derived surface water $[CO_3^{2-}]$ remains below modern concentrations across the glaciation.

$\delta^{13}C$ DERIVED $\Delta[CO_3^{2-}]$

Carbonate ion concentration changes derived from $\delta^{13}C$ across the glaciation range from -127 to 12.3 µmol/kg, with an average of -51.8 µmol/kg and a standard deviation of 24.4 µmol/kg (Fig. 5b). From the start of the record in an interglacial period at 95.5 kyr to the end in a glacial period at 70.2 kyr, there is a slight increase in $\Delta[CO_3^{2-}]$, however low sample abundance only allowed for two data points across the glacial portion of this climate transition. Thus, as with the $\delta^{13}C$ record in the glaciation, changes across glaciation are inconclusive.

Carbon isotope-derived $\Delta[CO_3^{2-}]$ steadies around -52.1 µmol/kg from the start of the record at 95.5 kyr to the beginning of MIS5b at 92.1 kyr. At this point, values decrease to the lowest point in all records at -127 µmol/kg at 91 kyr. Then, across MIS5b, $\Delta[CO_3^{2-}]$ steadily increases into early MIS5a where, between 83.7 and 81.9 kyr, values decrease 46.5 µmol/kg. Concentrations later level off across the rest of MIS5a around -38.1 µmol/kg until the onset of MIS4. As the climate transitions into a glacial period, $\Delta[CO_3^{2-}]$ increases slightly up to 12.3 µmol/kg at the end of the record at 70.2 kyr. This record reveals lower than modern $[CO_3^{2-}]$ values across the glaciation, with a possible excursion (not outside of error) above modern in MIS4.

EFFECTS OF ATMOSPHERIC *p*CO_2 ON SURFACE WATER $[CO_3^{2-}]$

I combine the B/Ca-based $[CO_3^{2-}]$ with changes due to atmospheric *p*CO_2 variability and plot this record in Fig. 7c. This accounts for the total change in local surface water $[CO_3^{2-}]$ ($\Delta[CO_3^{2-}]$) relative to predicted atmospheric *p*CO_2 equilibrium values. Values range from -134 to 9.0 µmol/kg with an average of -71.0 µmol/kg and a standard deviation of 27.2 µmol/kg. Across the deglaciation, $\Delta[CO_3^{2-}]$ averages -50.4 µmol/kg with a standard deviation of 30.1 µmol/kg. The lowest $\Delta[CO_3^{2-}]$ is in the LGM (-129 µmol/kg) and concentrations then increase during the deglaciation. Changes in $\Delta[CO_3^{2-}]$ show an increasing trend across H1, BA, and YD. Then, in the early Holocene, concentrations drop slightly but continue to increase in the mid and late Holocene. Average $\Delta[CO_3^{2-}]$ is -91.1 µmol/kg (n=5) across the glacial portion of the deglaciation (25 to 20 kyr), -53.9 µmol/kg (n=11) across the deglacial (20 to 11.5 kyr) portion, and -20.1 µmol/kg (n=8) across the interglacial, or Holocene, (11.5 kyr to present).

Across the glaciation, surface water $\Delta[CO_3^{2-}]$ concentrations remain fairly steady across the interglacial and glacial portion of the glaciation with an average of -79.1 µmol/kg and a

standard deviation of 21.0 µmol/kg. The interglacial portion (before 72 kyr) has an average $\Delta[CO_3^{2-}]$ of -76.2 µmol/kg, while the glacial portion (after 72 kyr) averages -92.4 µmol/kg, a 16.2 µmol/kg difference. Surface water $\Delta[CO_3^{2-}]$ is less variable across the glaciation than the deglaciation.

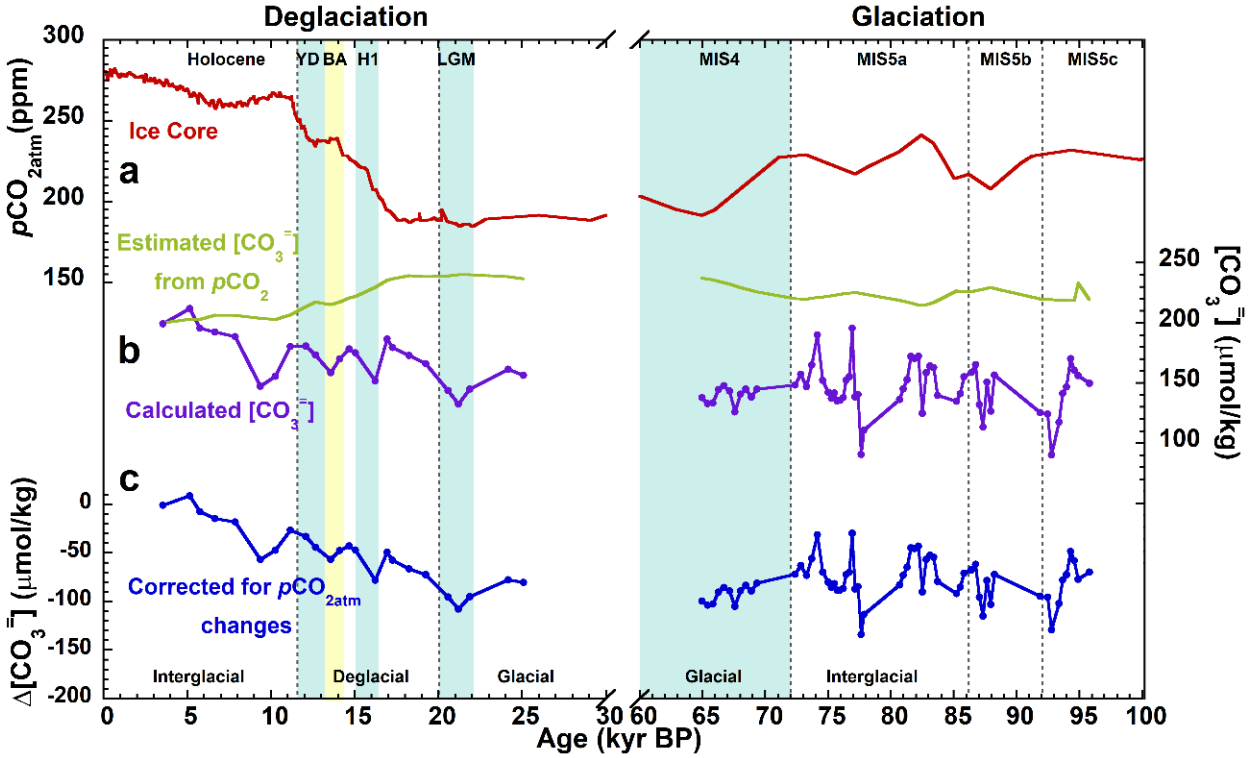

Figure 7. B/Ca derived $[CO_3^{2-}]$ (µmol/kg) corrected for temporal changes in atmospheric pCO_2. a) Atmospheric pCO_2 (ppm) from Dome C (Monnin et al., 2001) and Vostok Ice Core (Petit et al., 1999; Pépin et al., 2001; Raynaud et al., 2005). b) B/Ca reconstructed $[CO_3^{2-}]$ in µmol/kg is indicated in dark purple and $[CO_3^{2-}]$ estimated from changes in atmospheric pCO_2 in the green. c) B/Ca derived $\Delta[CO_3^{2-}]$ in µmol/kg with changes from atmospheric pCO_2 added, reflecting local surface water change relative to atmosphere. The gray dashed lines represent glacial-interglacial boundaries in the deglaciation and boundaries between Marine Isotope Stages in the glaciation.

CHAPTER IV

DISCUSSION

B/CA PROXY

Although the B/Ca : [CO_3^{2-}] proxy has been shown to be robust and well-established in benthic foraminifera (Yu & Elderfield, 2007; Yu et al., 2010), its reliability for reconstructing [CO_3^{2-}] using planktic foraminifera has been the subject of debate (Allen et al., 2011; Allen et al., 2012; Allen & Hönisch, 2012). Allen & Hönisch (2012) questioned the proposed control of foraminiferal boron uptake, seawater pH, and calibrations based on the boron partitioning coefficient, K_D, particularly because K_D is also influenced by both temperature and salinity (Allen & Hönisch, 2012; Foster, 2008; Yu et al. 2007). They advised against the use of the proxy in planktic foraminifera unless the influence of other parameters were better constrained.

Krupinski et al. (2017) followed up on the study by Allen & Hönisch (2012) and derived an empirical calibration for B/Ca : [CO_3^{2-}] for *G. bulloides*, while also carefully constraining the effects of other parameters. They used 37 core tops across the Pacific spanning a variety of carbonate chemistry conditions (e.g., pH, [CO_3^{2-}], $\Omega_{calcite}$) and a range of temperatures. In addition, they designated calcification depths for each *G. bulloides* location based on Mg/Ca or $\delta^{18}O$ temperature and then assigned each sample carbonate chemistry data based on calcification depth. They then measured B/Ca ratios and calculated the correlation between B/Ca ratios in *G. bulloides* and carbonate system parameters, finding a correlation between B/Ca and $\Omega_{calcite}$ and B/Ca and [CO_3^{2-}]. They found little or no correlation, however, between K_D and [CO_3^{2-}]. They, therefore, calibrated a new proxy based on the direct relationship of B/Ca and [CO_3^{2-}], rather than K_D. While Krupinski et al. (2017) resolved the mechanistic issue behind the B/Ca proxy,

complexities remain within proxy methodologies such as multiple *G. bulloides* morphotypes and low concentrations of boron in planktic foraminiferal tests.

The presence of multiple *G. bulloides* morphotypes with different B/Ca : [CO_3^{2-}] sensitivities complicate the use of the B/Ca proxy. While I was able to rule out the presence of the encrusted morphotype in the EEP using an area density analysis (see methodology), future analyses could be strengthened by using scanning electron microscopy (SEM) as an additional tool to visually identify encrusted *G. bulloides* by their decreased pore density and rougher surface structure (Krupinski et al., 2017; Osborne et al., 2016).

Another challenge with the B/Ca proxy in planktic foraminifera is that the concentration of boron in their tests is very low. As a result, B/Ca ratios in planktic foraminifera shells are much lower (~20 to 100 µmol/mol) than those found in benthic foraminifera (~150 to 275 µmol/mol) and thus more difficult to measure analytically (Yu & Elderfield, 2007). Because of these low boron concentrations, deposition of boron from the air, inadequately leached plastics, improperly filtered water, and various other factors can easily contaminate samples and alter results.

To overcome the obstacles caused by low boron concentrations in planktic foraminiferal tests, I meticulously worked to prevent boron contamination in the laboratory. All plastics, including vials and secondary containers for cleaning, were acid-leached with 10% HCl made with boron-free water and all standards and cleaning agents were created with boron-free water. Fume hoods and clean benches were cleaned and inspected for dust prior to use and trace element level clean lab gloves were used. For ICP-MS analysis, the instrument was optimized to measure very small quantities of boron. Also, ten 2% HNO_3 blanks instead of the typical three were run prior to each ICP-MS run in order to clean out any residual boron in the system. Lastly,

all vials containing dissolved samples and standards were opened in sets of five in order to avoid deposition of boron from the air (the "fall-in effect") (Rae et al., 2011).

$\delta^{13}C$ PROXY

Spero et al. (1999) first described the $\delta^{13}C$: $\Delta[CO_3^{2-}]$ proxy and explained its mechanisms and reliability. *G. ruber* and *T. sacculifer* are both symbiont-bearing planktic foraminifera species and have similar seasonal growth patterns and depth habitats, which means these influences should impact their $\delta^{13}C$ values similarly. Nevertheless, he found that the change in shell $\delta^{13}C$ relative to ambient $[CO_3^{2-}]$ differs between the two species. Therefore, this allows for $[CO_3^{2-}]$ to be reconstructed based on the $\delta^{13}C$ differences between the two species when measured in the same sediment core interval. However, utilization of two species for one data point amplifies uncertainties because slight habitat depth differences between species could lead to errors. Moreover, the proxy is based on many assumptions: 1) that both *T. sacculifer* and *G. ruber* record $\delta^{13}C$ of the seawater equally; 2) that any effects of dissolution would affect both species the same; 3) that the carbonate chemistry of the seawater is constant across the entire calcification depth of both species (up to ~100 m for *T. sacculifer*); and 4) that the slope of $\delta^{13}C$ change vs. $[CO_3^{2-}]$ change for each species is constant through time. Calibration of $\Delta[CO_3^{2-}]$ from $\delta^{13}C$ is also complex, involving multiple equations, which both complicates and compounds the resulting error (see methodology).

$\Delta[CO_3^{2-}]$ RECORD COMPARISION

Remarkably, both the B/Ca- and $\delta^{13}C$-derived $\Delta[CO_3^{2-}]$ records display similar patterns across portions of the deglaciation and glaciation (Fig. 8). Across the deglaciation, both records generally remain within error of each other. They show increases in $\Delta[CO_3^{2}]$ across the last deglaciation and into the interglacial. Modern core-top values of both records are also similar

and produce a 2 µmol/kg difference in $\Delta[CO_3^{2-}]$ between 4.95 and 5.15 kyr. There are divergences in the records, however, in the glacial portion of the record and in the mid-Holocene, where the records differ outside of the estimated error. In the glacial portion, the B/Ca-derived record shows low $\Delta[CO_3^{2-}]$ and suggests the EEP was a greater source of CO_2 to the atmosphere Conversely, the $\delta^{13}C$-derived record indicates the EEP was less of a source of CO_2 across this time. In the mid-Holocene, reconstructed $\Delta[CO_3^{2-}]$ diverges with an increase in B/Ca-derived $\Delta[CO_3^{2-}]$ indicating less CO_2 outgassing and a decrease in $\delta^{13}C$-derived $\Delta[CO_3^{2-}]$ indicating greater CO_2 outgassing. Quantitatively, the two proxy records show weak correlation across the deglaciation (Pearson's, r=-0.20).

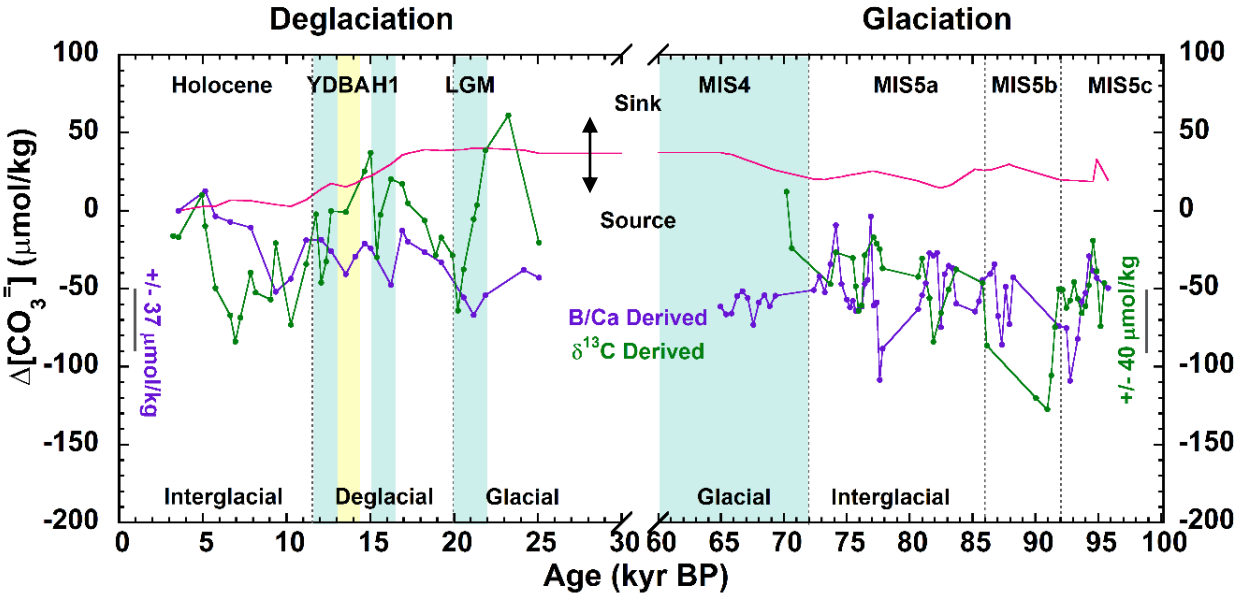

Figure 8. Complete $\Delta[CO_3^{2-}]$ (µmol/kg) reconstruction across the deglaciation and glaciation. $\Delta[CO_3^{2-}]$ calculated from $\delta^{13}C$ in *T. sacculifer* and *G. ruber* is represented in green with an error of $\pm$ 40 µmol/kg) and $\Delta[CO_3^{2-}]$ calculated from B/Ca from *G. bulloides* in purple with an error of $\pm$ 37 µmol/kg. The pink line is the estimated change in surface water $[CO_3^{2-}]$ based on temporal changes in atmospheric pCO_2 alone. The gray dashed lines represent glacial-interglacial boundaries in the deglaciation and boundaries between Marine Isotope Stages in the glaciation.

Across the entirety of the glaciation from 96 to 60 kyr, both records remain within error of each other, reveal lower than modern surface water $\Delta[CO_3^{2-}]$, and suggest greater CO_2 outgassing (Fig. 8). Despite an inability to distinguish differences outside of error between records, the two records show no correlation with one another (Pearson's, r=0.03).

Offsets in depth habitats between the planktic foraminiferal species used in both proxies could account for part of the discrepancies between records. While all three species are most abundant in the upper mixed layer within the top 25 m of the water column in the Panama Basin (Bé et al., 1985; Fairbanks et al. 1982), *G. bulloides* is associated with upwelling conditions and is often found closer to 25 m owing to its colder-water preference (Fairbanks et al. 1982; Kretschmer et al., 2017; Thunell & Reynolds, 1984). This could cause differences in the records due to slight water column variations in carbonate chemistry. Additionally, because *G. bulloides* are considered an upwelling species, the B/Ca-derived record might record changes in upwelling undetected by *G. ruber* and *T. sacculifer* in the $\delta^{13}C$ proxy.

Furthermore, seasonal differences in the abundance between species could also cause inconsistencies between records. Seasonal shifts in foraminiferal abundance driven by food availability and temperature changes were first noted in Bé (1960) and further explored in numerous studies since (Eguchi et al., 1999; Kawahata et al., 2002; Kretschmer et al., 2017; Thunell & Reynolds, 1984; Tolderlund & Bé, 1971). A study conducted by Thunell & Reynolds (1984) used sediment traps at various depths in the Panama Basin and revealed that *G. ruber, T. sacculifer,* and *G. bulloides* all have large peaks in abundance in July-August. They also found that *G. ruber* and *T. sacculifer* have a smaller secondary spike in January-February, while *G. bulloides* have a secondary peak slightly later in March-April. This difference in secondary abundance peaks could create an offset in the data because, despite both the B/Ca- and $\delta^{13}C$-

derived records recording the same age, the *G. bulloides* could record slightly different [CO_3^{2-}] than *G. ruber* and *T. sacculifer*.

Another factor that could cause the records to differ is the required normalization of the B/Ca-derived [CO_3^{2-}] to core-top values to produce comparable data. The B/Ca proxy produces surface water [CO_3^{2-}], while the $\delta^{13}C$ proxy produces a record of *changes* in [CO_3^{2-}] ($\Delta[CO_3^{2-}]$) downcore. In order for both records to represent the same parameter and to accurately compare them, I subtracted the core top B/Ca-derived [CO_3^{2-}] value from each subsequent data point to produce values representing changes in [CO_3^{2-}] downcore. Although this allowed for an appropriate comparison, the proxy calibrations themselves initially produced slightly different surface water carbonate ion parameters that would not have otherwise been directly comparable. Additionally, because the B/Ca proxy produced [CO_3^{2-}] rather than $\Delta[CO_3^{2-}]$, I was able to remove concentration changes due to atmospheric pCO_2. Henceforth, I focus interpretation and comparison efforts primarily on the B/Ca-derived record corrected for temporal changes in atmospheric pCO_2.

ADDRESSING HYPOTHESES

To investigate the cause of the lower-than-modern surface water [CO_3^{2-}] seen across both glacial transitions, I address the dominant influences on surface seawater [CO_3^{2-}]. Surface water [CO_3^{2-}] is controlled by total DIC and pH, where DIC is equal to:

$$DIC = [CO_2] + [HCO_3^-] + [CO_3^{2-}] \text{ (Zeebe, 2012).} \quad [6]$$

Many environmental mechanisms that control components of DIC also influence pH. These factors include atmospheric pCO_2, salinity, total alkalinity, productivity, and upwelling. Furthermore, these parameters are all connected to each other and to surface water [CO_3^{2-}] (Hönisch & Hemming, 2002; Sanyal et al., 1995; Sigman & Boyle, 2000). Surface water

absorption of CO_2 due to decreased ocean-atmosphere partial pressure from glacial-interglacial atmospheric pCO_2 fluctuations cause significant shifts in surface water $[CO_2]$, however, I accounted for this influence on surface water $[CO_3^{2-}]$ (Fig. 7).

Salinity plays a role in surface water $[CO_2]$, as well, because an increase in salinity causes decreased dissolved gas solubility, decreased $[CO_2]$, increased pH, and increased $[CO_3^{2-}]$ (Sigman & Boyle, 2000; Zeebe, 2012). Could a large local salinity decrease have caused increased $[CO_2]$ and decreased $[CO_3^{2-}]$ during the glaciation and deglaciation? Lea et al. (2000, 2002) used Mg/Ca temperatures and $\delta^{18}O$ in *G. ruber* to reconstruct variations in sea surface temperature (SST) and $\delta^{18}O_{seawater}$ between the eastern and western equatorial Pacific over the last 350 kyr. They found that $\delta^{18}O_{seawater}$ variability in the EEP was consistent with global changes in $\delta^{18}O_{seawater}$ caused by ice volume variability. Because the magnitude of $\delta^{18}O_{seawater}$ change in EEP matched that of the global ocean across the last glacial cycle, it can be concluded that the EEP did not experience significant changes in salinity across the last several glacial cycles. This eliminates increased salinity as the cause of observed low $[CO_3^{2-}]$ values across both glacial transitions.

Next, decreased alkalinity could account for low surface water $[CO_3^{2-}]$. Total alkalinity (TA) is defined as:

$$TA = [HCO_3^-] + 2[CO_3^{2-}] + [OH^-] - [H^+]. \quad [7]$$

In seawater, TA is dominated by $[HCO_3^-]$ and $[CO_3^{2-}]$ (Wolf-Gladrow et al., 2007). Over half of seawater alkalinity variance is driven by changes in salinity, with the other half driven by calcification and carbonate dissolution processes (Hönisch & Hemming, 2002). As discussed above, it was shown that the EEP did not experience large salinity changes on glacial-interglacial timescales (Lea et al., 2000, 2002). If alkalinity changes were to occur in the region on a scale

large enough to significantly alter [CO_3^{2-}], it would have to be driven by substantial changes in carbonate precipitation/dissolution. Namely, an increase in precipitation would have had to occur because it decreases TA through HCO_3^- removal (Zeebe et al., 2012). While there are few studies that look at calcite precipitation changes in the past in the EEP, Martínez-Botí et al. (2015) modeled TA changes in the region across the last deglaciation and found that TA had little influence on seawater pCO_2 estimates, suggesting changes in TA had little influence on [CO_3^{2-}] over the last glacial cycle. Therefore, neither changes in salinity nor TA can explain the lower glacial [CO_3^{2-}] in my records.

CARBONATE SYSTEM CHANGES IN THE EEP ACROSS THE DEGLACIATION AND GLACIATION

Martínez-Botí et al. (2015) used boron isotopes as a proxy for pH, along with Mg/Ca temperatures and estimates of alkalinity and salinity, to reconstruct seawater pCO_2 and, thus, ΔpCO_{2sw} in the EEP across the last deglaciation in core ODP1238 (Fig. 2). The speciation of $^{11}B/^{10}B$ is controlled by seawater pH and, therefore, it can be used as a paleo-pH proxy (Foster, 2008). On the other hand, the ratio of Mg/Ca in foraminifera is a temperature proxy, driven by Mg partitioning during calcification (Elderfield & Ganssen, 2000). Martínez-Botí et al. (2015) coupled these proxies with salinity estimates from changes in ice volume (Schmidt, 1999) and alkalinity based on modeling studies to calculate seawater pCO_2 using statistical software. Because it is possible to reconstruct the carbon system from two of the six carbonate system parameters, as well as temperature, salinity, and depth, they calculated the remaining carbon cycle components including ΔpCO_{2sw} (Zeebe & Wolf-Gladrow, 2001). Oceanic ΔpCO_{2sw} represents the partial pressure difference of pCO_2 between the ocean and atmosphere. When ΔpCO_{2sw} is negative, it denotes that the pCO_2 of the ocean is less than that of the atmosphere and

indicates oceanic absorption of CO_2. It also suggests increased surface water pH and, therefore, increased [CO_3^{2-}]. When ΔpCO_{2sw} is positive, it indicates greater pCO_2 in the ocean than in the atmosphere, oceanic CO_2 outgassing, higher seawater [CO_2], lower pH, and decreased [CO_3^{2-}].

Martínez-Botí et al. (2015) found decreased ΔpCO_{2sw} across the LGM in the EEP, which suggested the region switched from being a source to a sink of CO_2 in the past (Fig. 9). They theorized that increased dust flux associated with the cold, dry glacial climate stimulated the biological pump, which in turn caused the region to become a sink for atmospheric CO_2. One of the goals of my study was to test this hypothesis and reconstruct changes in the carbon system at a nearby core across the deglaciation. If B/Ca reconstructed surface water [CO_3^{2-}] was higher compared to the modern across the glacial portion of the last 25 kyr, this would validate the theory posed by Martínez-Botí et al. (2015) and suggest that CO_2 outgassing across the EEP is sensitive to changes in productivity. Our results, however, fail to replicate the switch from source to sink shown by Martínez-Botí et al. (2015) and instead suggest the EEP was a greater source of CO_2 to the atmosphere during the LGM and across the deglaciation (Fig. 9).

Converse to the ΔpCO_2 record from Martínez-Botí et al. (2015), the B/Ca-derived [CO_3^{2-}] record from 17JC suggests greater CO_2 outgassing across the LGM and indicates the region may have been an even greater source of CO_2 to the atmosphere than today (Fig. 9). This is also contrary to the common understanding that global oceanic [CO_3^{2-}] increases across glacial periods (Hönisch & Hemming, 2005; Zeebe, 2012). Nevertheless, local decreases in surface water [CO_3^{2-}] could occur simultaneous to global increases, similar to how the modern global ocean acts as a net CO_2 sink, but the EEP acts as a source today. Site ODP1238 is located to the east of 17JC and therefore may have experienced less upwelling during the LGM and/or a greater dust flux, which could have delivered more nutrients and stimulated greater productivity.

It is possible that the net balance between upwelling, dust delivery, biological productivity, and carbon flux is variable and subject to regional heterogeneity, which could be the reason for the difference between the ΔpCO_{2sw} from ODP1238 and surface water $[CO_3^{2-}]$ at 17JC.

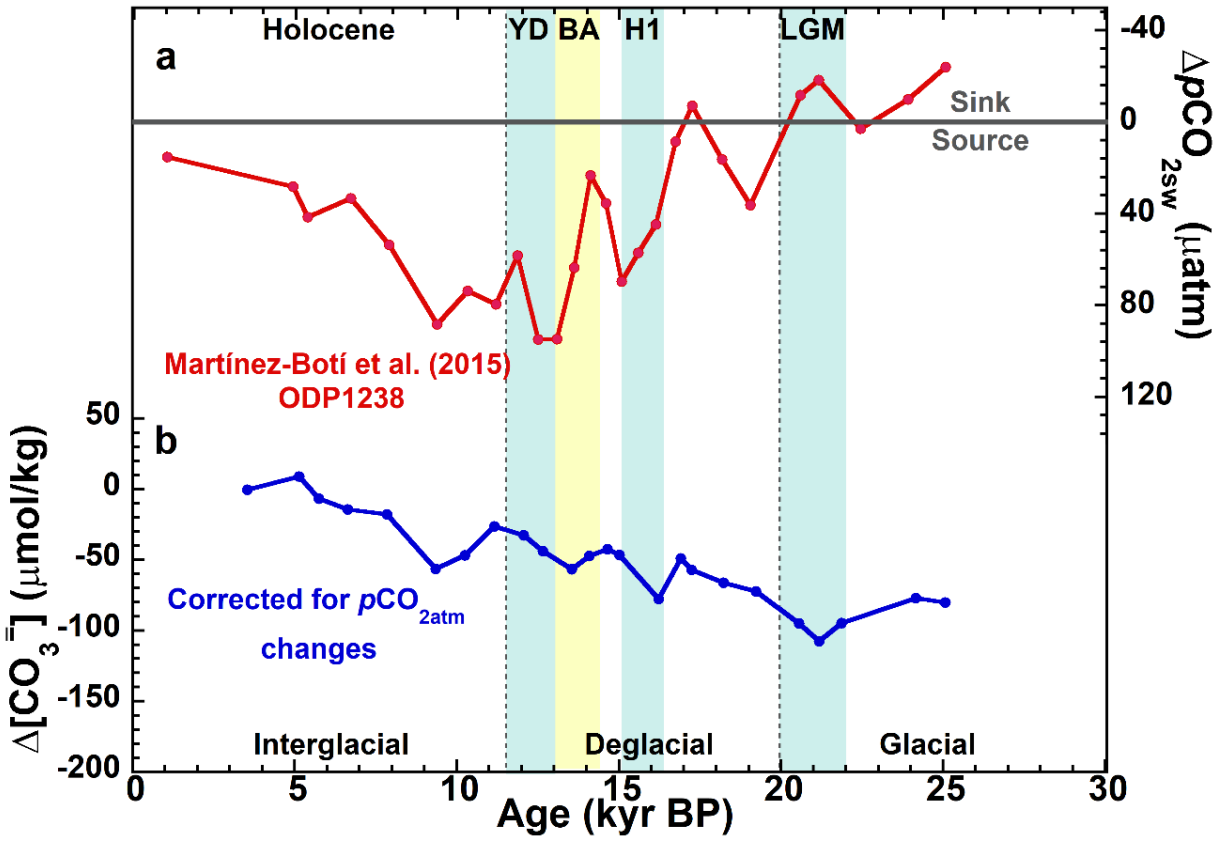

Figure 9. Martínez-Botí et al. (2015) proxy comparison. a) ΔpCO_{2sw} (µatm) from Martínez-Botí et al. (2015) at ODP site 1238. b) B/Ca derived $\Delta[CO_3^{2-}]$ from 17JC in µmol/kg with changes from atmospheric pCO_2 included, reflecting total changes in local seawater $[CO_3^{2-}]$. The gray dashed line represents the boundary between glacial, deglacial, and interglacial climate.

Loveley et al. (2017) used ^{232}Th and xsBa as proxies for dust flux and export production, respectively, in the EEP in core 17JC, the same core used in this study (Fig. 11a and b). The ^{232}Th proxy is a tracer for windblown continental dust due to the isotopic signature of eolian dust (Francois et al., 2004; Winckler et al., 2008). Loveley et al. (2017) found that the isotopic signature of ^{232}Th in 17JC indicated that it was nearly all derived from windblown dust. They corroborated this by $^{234}U/^{238}U$ measurements in bulk sediment. While ^{234}U is authigenic, ^{238}U in seawater is due to eolian input, therefore deviations in the ratio suggest dust delivery. Next, they measured the difference between authigenic barium and barium from organic matter in their samples (xsBa), as a proxy for changes in export production and, therefore, primary productivity.

Loveley et al. (2017) found increases in dust flux and increases in biological productivity occurred simultaneously during cold Heinrich events of the last 80 kyr in the region. They theorized that iron fertilization from increased dust delivery when the ITCZ shifted southward during Heinrich events increased the efficiency of the biological pump and may have reduced CO_2 outgassing. My study sought to further explore this hypothesis, which would be strengthened if surface water $[CO_3^{2-}]$ values increased across Heinrich events coeval with increases in dust flux.

Nevertheless, the B/Ca-derived surface water $[CO_3^{2-}]$ record does not show substantial increases correlated to either the ^{232}Th or xsBa records from Loveley et al. (2017) across the last glacial and deglacial periods (Fig. 10 a,b,d). The B/Ca-derived surface water $[CO_3^{2-}]$ record does not correlate with peaks in dust flux and export production seen by Loveley et al. (2017) across Heinrich events 9 through 7 and H1 (Fig. 10 a,b,d). Increases in surface water $[CO_3^{2-}]$ occur across H8 and H1, however the increases are minimal (36.6 µmol/kg and 31.1 µmol/kg, respectively) and not large enough to suggest a significant shift in the surface seawater carbonate

chemistry at 17JC. Taken at face value, this suggests that pulses of dust fluxes across cold, dry Heinrich events in the region did not increase productivity enough to cause the EEP to become a net CO_2 sink.

Spero (unpublished data) used the $\delta^{13}C$ differences between *G. ruber* and *T. sacculifer* as a proxy for $\Delta[CO_3^{2-}]$ (see methodology) in core TR163-19, to the northeast of 17JC. He found a large increase in $\Delta[CO_3^{2-}]$ across the last glaciation from 96 to 60 kyr and hypothesized that a prominent shift in the EEP carbon cycle may have occurred across this transition due to changes in productivity or upwelling. With evidence from Loveley et al. (2017) suggesting iron fertilization and associated stimulated biological productivity across cold periods in the EEP, I sought to determine if surface water $\Delta[CO_3^{2-}]$ increased in 17JC across this transitional climate period. If reconstructed $\Delta[CO_3^{2-}]$ from core 17JC showed a similar pattern of increase to that of Spero (unpublished), then perhaps changes in CO_2 outgassing due to iron fertilization occurred often in the past across glacial transitions in the EEP.

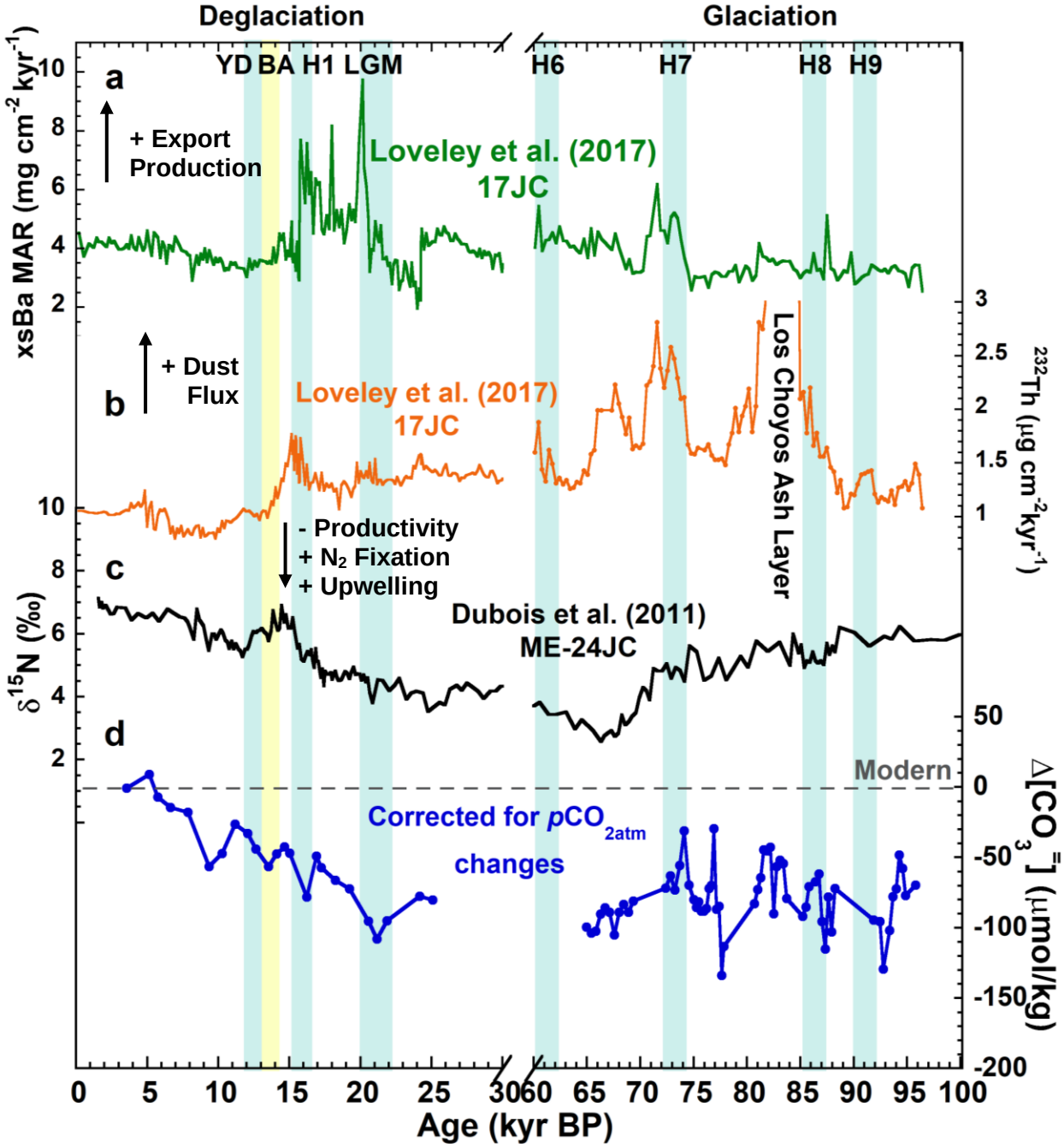

Figure 10. Carbonate ion concentration record comparison. a) xsBa mass accumulation rates (MAR, mg $cm^{-2}kyr^{-1}$) from Loveley et al. (2017) in core 17JC as a proxy for export productivity. b) ^{232}Th flux (µg $cm^{-2}kyr^{-1}$) from Loveley et al. (2017) from core 17JC as a proxy for dust flux. c) $\delta^{15}N$ from Dubois et al. (2011) from core ME0005A-24JC (0º01.30'N 86º27.79'W, 2941 m) as an upwelling and productivity indicator. d) B/Ca derived $\Delta[CO_3^{2-}]$ in µmol/kg relative to equilibrium atmospheric pCO_2 concentration. The gray dashed lines represent glacial-interglacial boundaries in the deglaciation and boundaries between Marine Isotope Stages in the glaciation.

A comparison between the Spero (unpublished) record from Cocos Ridge core TR163-19 and the $\delta^{13}C$ derived $\Delta[CO_3^{2-}]$ record from 17JC is shown in Fig. 11. While both records show an increase in $\Delta[CO_3^{2-}]$ from 90 to 69 kyr, Spero (unpublished)'s record rises more rapidly from 81 to 70 kyr and indicates a greater shift in the carbon system than the record from 17JC. The B/Ca-derived $\Delta[CO_3^{2-}]$ record from 17JC, however, fails to demonstrate an increase such as that shown in the Spero (unpublished) record. Ultimately, while our $\delta^{13}C$-derived $\Delta[CO_3^{2-}]$ record shows potentially increased $\Delta[CO_3^{2-}]$ similar to Spero (unpublished), the B/Ca-derived record fails to corroborate this result.

Resolution differences, lack of sample, and latitudinal offsets could explain inconsistences between $\delta^{13}C$-derived $\Delta[CO_3^{2-}]$ records, while depth and seasonal offsets complicates inter-proxy comparison. Core 17JC is higher resolution than TR163-19 and therefore records finer variation in seawater carbonate chemistry. Furthermore, the 17JC $\delta^{13}C$-derived record has limited data points in MIS4 due to low species abundance which limits the glacial period comparison. More data points in MIS4 could reveal a greater increase in $\Delta[CO_3^{2-}]$ and better corroborate Spero (unpublished), however species abundance was significantly limited across this time frame. Comparison of the B/Ca-derived $\Delta[CO_3^{2-}]$ record from 17JC and the $\delta^{13}C$-derived $\Delta[CO_3^{2-}]$ record from TR163-19 is complicated by the same obstacles that arise with the inter-proxy comparison in this study. Depth and seasonal offsets between species, as well as required normalization of the B/Ca proxy could cause inconsistencies in records. In comparison of all records, geographic differences between cores could produce conflicting results. Core TR163-19 is to the northeast of 17JC and located just north of the cold upwelling water that typically characterizes the EEP, therefore increases in surface water $[CO_3^{2-}]$ that occur

at TR163-19 could be damped at 17JC due to increased upwelling of CO_2-rich waters (Spero & Lea, 2002).

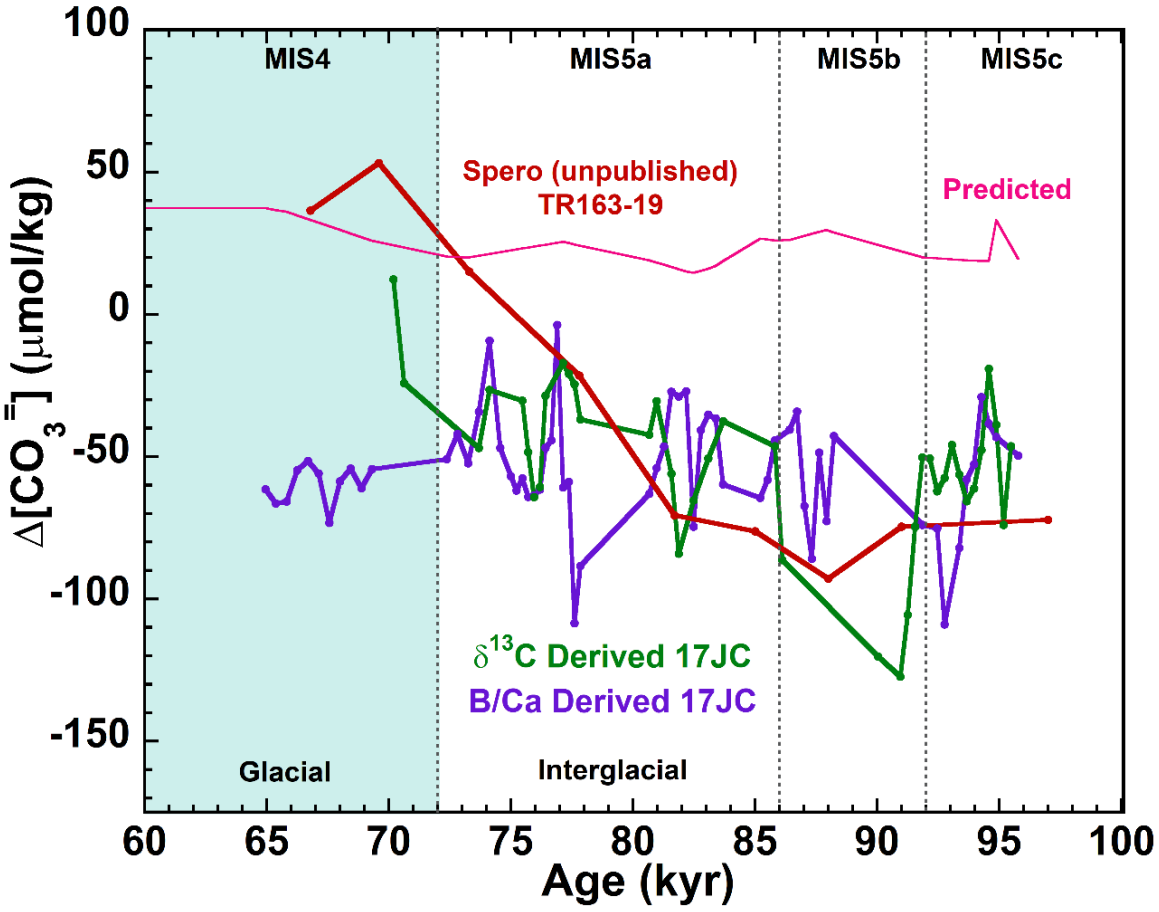

Figure 11. Comparison of $\Delta[CO_3^{2-}]$ (µmol/kg) records from 17JC and TR163-19. $\delta^{13}C$-derived $\Delta[CO_3^{2-}]$ from core TR163-19 from Spero (unpublished) is in red, $\delta^{13}C$-derived $\Delta[CO_3^{2-}]$ from core 17JC in green, and B/Ca-derived $\Delta[CO_3^{2-}]$ from core 17JC in purple. The pink line is the calculated surface water $[CO_3^{2-}]$ change relative to atmospheric pCO_2. The gray dashed lines represent boundaries between Marine Isotope Stages.

CAUSES FOR PAST CHANGES IN SURFACE WATER [CO_3^{2-}] IN THE EEP

Surface water pH has a direct relationship to [CO_3^{2-}], with decreased pH driving down [CO_3^{2-}]. Because changes in DIC cannot explain lower-than-modern surface water [CO_3^{2-}] in the EEP across the deglaciation and glaciation, decreased local pH driven by local upwelling could explain my results. Previous studies found evidence for enhanced upwelling in the EEP, particularly from 17 to 10 kyr during the deglaciation, denoted as the last glacial termination (Anderson et al., 2009; Chase et al., 2002; Dubois et al., 2011; Haynes et al., 2011), and from 74 to 70 kyr across the glaciation (Dubois et al., 2011; Haynes et al., 2011; Pena et al., 2008).

Nitrogen isotopes measured in bulk marine sediments can be used as an indicator for both upwelling, productivity, and nitrogen fixation. Deep waters have a low $^{15}N/^{14}N$ ratio due to accumulation of respired nutrients. Therefore, low $\delta^{15}N$ suggests increased upwelling of deep waters (Dubois et al., 2011; Kienast et al., 2002). Moreover, because an increase in productivity leads to an increase in denitrification, and denitrification isotopically favors ^{14}N, higher $\delta^{15}N$ ratios suggest increases in productivity. On the other hand, iron-limited nitrogen fixation by diazotrophs introduces isotopically light nitrogen and leaves a lighter isotopic signature (Brandes et al., 1998; Somes et al., 2010). Therefore, nitrogen isotopes reflect a balance between upwelling and productivity (denitrification) because increased upwelling drives down $\delta^{15}N$ but also stimulates productivity that increases $\delta^{15}N$. This is further complicated, particularly in the EEP, across periods of iron fertilization with increased dust flux stimulating both denitrification and nitrogen fixation leaving heavier and lighter surface water isotopic signatures, respectively (Brandes et al., 1998; Somes et al., 2010). Figure 11c shows $\delta^{15}N$ (‰) from Dubois et al. (2011) from core ME0005A-24JC.

The Dubois et al. (2011) $\delta^{15}N$ record in the EEP shows increased upwelling in the glacial portion of the deglaciation, with greatest upwelling in the LGM, and a decreasing trend into the Holocene. Across the glaciation, the $\delta^{15}N$ record indicates a similar pattern, with enhanced upwelling in the glacial portion and decreased upwelling in Holocene. The record also shows lower $\delta^{15}N$ across the entire glaciation when compared to the modern, suggesting upwelling was more enhanced across the glacial period. Given this evidence, I propose that enhanced upwelling of CO_2- and nutrient-rich deep water may have decreased surface water pH and $[CO_3^{2-}]$, particularly across the deglaciation. However, because of the large magnitude of surface water $[CO_3^{2-}]$ decrease across both glacial transitions, enhanced upwelling alone cannot explain all of the change.

To further investigate the drivers of low surface water $[CO_3^{2-}]$, I compare my records to a proxy for bottom water oxygenation in the Panama Basin. Loveley et al. (2017) measured authigenic U in 17JC sediments as a proxy for bottom water oxygen content (Fig. 12a). Authigenic U is controlled by export production and oxygen content of bottom waters (Loveley et al., 2017). They found that bottom waters were most depleted in oxygen at the LGM and increased in oxygen content across the deglaciation and into the Holocene. This trend is similar to that of the surface water $[CO_3^{2-}]$ record, with the lowest $[CO_3^{2-}]$ in the LGM and highest in the Holocene, increasing from glacial to interglacial climate (Fig. 12a,c). The surface water $[CO_3^{2-}]$ record shows a strong correlation (Pearson's, r=0.84) with bottom water O_2 content, which suggests upwelling of low O_2, high CO_2 bottom water may have influenced surface water carbonate chemistry.

In addition, Close (2020) used B/Ca in benthic foraminifera as a proxy for bottom water $[CO_3^{2-}]$ in 17JC (Fig. 12b). The B/Ca proxy in benthic foraminifera, just as the B/Ca proxy used

here, is based on the relationship between [CO_3^{2-}] and $\Omega_{calcite}$, with increased B/Ca increasing with [CO_3^{2-}] (Yu & Elderfield, 2007). Close (2020) found that bottom water [CO_3^{2-}] was lowest in the LGM, with concentrations increasing across the deglaciation and into the Holocene (Fig. 12b). He found that a poorly ventilated water mass source along with increased surface water productivity likely increase carbon storage inside the Panama Basin during the glacial period. Although the magnitude of change of the bottom water [CO_3^{2-}] (~31 µmol/mol) across the deglaciation is about four times less than that of surface water [CO_3^{2-}] in this study (~117 µmol/mol), the records share similar patterns. The two records exhibit a strong correlation (Pearson's, r=0.70), with decreased bottom water [CO_3^{2-}] corresponding to decreased surface water [CO_3^{2-}]. Therefore, the accumulation of CO_2-rich waters inside the Panama Basin as a whole during the glacial period may have reduced the [CO_3^{2-}] of upwelled waters and contributed to the low surface water [CO_3^{2}] recorded at 17JC.

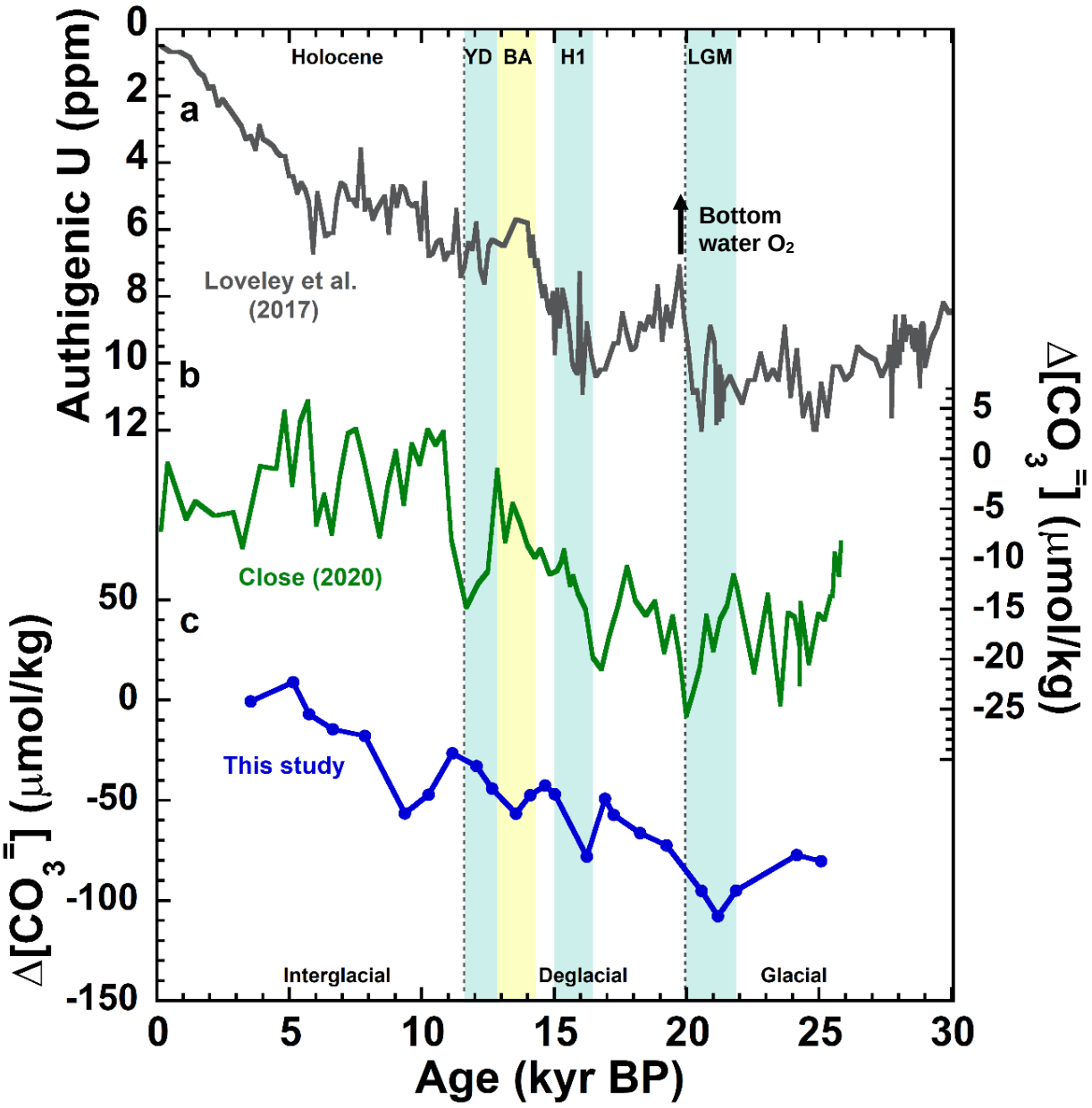

Figure 12. Bottom water comparisons in 17JC across the deglaciation. a) Authigenic U (ppm) from Loveley et al. (2017) in core 17JC as a proxy for bottom water oxygenation. b) $\Delta[CO_3^{2-}]$ reconstruction from benthic B/Ca ratios from Close (2020) in 17JC. c) B/Ca derived $\Delta[CO_3^{2-}]$ in µmol/kg with changes from atmospheric pCO_2 removed, reflecting local changes in seawater chemistry. The gray dashed line represents boundaries between glacial, deglacial, and interglacial climate.

These records all suggest a connection between low-oxygen, low-[CO_3^{2-}] subsurface water and decreased surface water [CO_3^{2-}] across the deglaciation, but because of the larger magnitude of change in surface water Δ[CO_3^{2-}] compared to the deep waters, there must be an additional source of CO_2-rich water to the surface. The oxygen minimum zone (OMZ) in the EEP is notable for its size and degree of hypoxia owing to high surface production, a sharp pycnocline that prevents ventilation, and slow circulation and old age of deep-water circulation in the region (Fielder & Talley, 2006). Oxygen depletion occurs at depths between productive surface waters and intermediate waters within the EEP today, between 350 and 400 m (Fielder & Talley, 2006). Proxy reconstructions suggest an expansion of the OMZ in the EEP across the deglaciation, likely driven by increased nutrient delivery to surface waters and subsequent increases in productivity and carbon export (Cartapanis et al., 2011; Martinez & Robinson, 2010; Robinson et al., 2009).

Hoogakker et al. (2018) used I/Ca ratios in planktic foraminifera as a proxy for upper water column oxygenation in the EEP across the last 40 kyr. The I/Ca proxy is based on the speciation of I in oxygenated water. Iodide (I^-) is the dominant species in low-oxygen waters (OMZs), while iodate (IO_3^-) dominates in well-oxygenated waters (Chance et al., 2010; Hoogakker et al., 2018). Because foraminiferal calcite only incorporates iodate, the ratio of I/Ca in tests changes with ambient O_2 levels. Therefore, lower I/Ca ratios reflect oxygen depleted waters. Hoogakker et al. (2018) measured I/Ca ratios in three foraminiferal species from ODP849 in the EEP: *N. dutertrei* and *P. obliquiloculata*, which dwell at or below the thermocline, and *T. sacculifer* which dwells in the surface mixed layer (Fairbanks et al., 1982). They found consistently low I/Ca across the last glacial period, which indicated decreased upper-ocean oxygen content and intensification of the OMZ in the region (Fig. 13a). Specifically, I/Ca

ratios less than 2.5 µmol/mol in core ODP849 indicate oxygen depleted waters in the upper 400 m of the water column in the EEP (Fig. 13a). They proposed that weak ocean circulation and increased productivity driven by a supply of nutrient-rich deep waters and enhanced upwelling contributed to the expansion of the OMZ across the last glacial period.

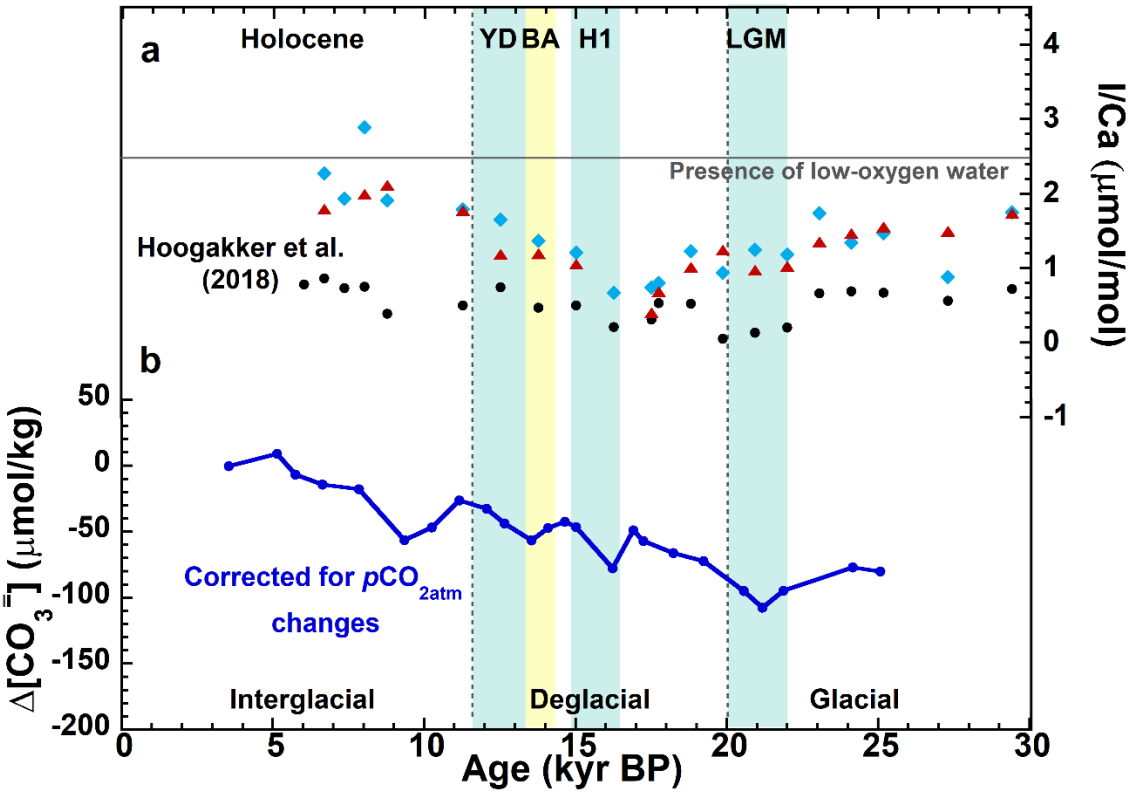

Figure 13. I/Ca ratios in planktic foraminifera from Hoogakker et al. (2018). a) I/Ca of *T. sacculifer* (red triangles), *P. obliquiloculata* (blue diamonds), and *N. dutertrei* (black circles) from Hoogakker et al. (2018) from core ODP849 (0.18° N, 110.50° W, 38500 m). b) B/Ca derived $\Delta[CO_3^{2-}]$ in µmol/kg with changes from atmospheric pCO_2 included, reflecting local changes in seawater chemistry. The gray dashed line represents boundaries between glacial, deglacial, and interglacial climate.

An expansion of the OMZ in the EEP would result in the accumulation of CO_2-rich intermediate waters below my study site and affect the carbonate chemistry of the source waters feeding the equatorial upwelling zone. The vertical transport of these CO_2-rich intermediate waters would have brought low pH, CO_2-rich waters to the surface at 17JC. As a result, surface water [CO_3^{2-}] would decrease. Therefore, it is likely that a combination of increased carbon storage inside the Panama Basin (Close 2020), increased upwelling (Dubois et al., 2011), and a decrease in source water [CO_3^{2-}] supplying the upwelling zone due to an expanded OMZ (Hoogakker et al., 2018) all worked together to decrease surface water [CO_3^{2-}] across the last glacial cycle.

CHAPTER V

CONCLUSION

Reconstructed surface water [CO_3^{2-}] using B/Ca ratios in *G. bulloides* and $\delta^{13}C$ in *G. ruber* and *T. sacculifer* from core 17JC indicates that the EEP largely remained a source of CO_2 to the atmosphere across the last deglaciation and last glaciation. I removed the influence of atmospheric pCO_2 changes on surface water [CO_3^{2-}] and the resulting record reveals lower-than-modern [CO_3^{2-}] across both climate transitions, which contradicts the hypotheses I set forth to test.

My results do not support the hypothesis that the EEP experienced a large increase in surface water [CO_3^{2-}] at the onset of the last glacial cycle. Also, converse to the ΔpCO_2 record from Martínez-Botí et al. (2015), the B/Ca-derived [CO_3^{2-}] record suggests greater CO_2 outgassing across the LGM and a decrease to the modern across the deglaciation. Compared to the Loveley et al. (2017) records, increased dust flux and productivity suggested by ^{232}Th and xsBa do not appear to overcome low surface water [CO_3^{2-}]. However, authigenic U records from Loveley et al. (2017) and bottom water [CO_3^{2-}] records from Close (2020) do correlate with surface water [CO_3^{2-}], indicating that increased carbon storage in the Panama Basin during the glacial period may have influenced surface water [CO_3^{2-}] in the past. Furthermore, $\delta^{15}N$ from Dubois et al. (2011) at a nearby core suggests increased upwelling across the deglaciation and increased productivity across the glaciation, which may have expanded the OMZ and increased the respired carbon content of intermediate depth source waters for the upwelling zone in the EEP.

I conclude that increased upwelling of both oxygen-depleted and CO_2-rich bottom and intermediate waters delivered high concentrations of CO_2 to the surface ocean and decreased [CO_3^{2-}] at 17JC. In the future, a surface water pH, I/Ca, and $\delta^{15}N$ record for core 17JC would help determine if, indeed, increased upwelling coupled with increased productivity across the last two glacial transitions caused decreased surface water [CO_3^{2-}].

Current rates of increase of atmospheric CO_2 far exceed those found on natural timescales. To predict how our climate system will respond in the future to sustained rapid carbon emissions, it is crucial to understand how components of the carbon cycle responded to climate perturbations in the past. Although I examine past behavior of a single component within the climate network, understanding the intricacies of each component is essential in order to fully grasp the system as a whole. Ultimately, I find the EEP, a significant part of the carbon cycle today, remained a source of CO_2 across the last two glacial transitions and suggest it may continue to do so in the future as anthropogenic carbon emissions continue to alter the global carbon cycle.

REFERENCES

Allen, K. A., & Hönisch, B. (2012). The planktic foraminiferal B/Ca proxy for seawater carbonate chemistry: A critical evaluation. *Earth and Planetary Science Letters, 345–348*, 203–211. https://doi.org/10.1016/j.epsl.2012.06.012

Allen, K. A., Hönisch, B., Eggins, S. M., Yu, J., Spero, H. J., & Elderfield, H. (2011). Controls on boron incorporation in cultured tests of the planktic foraminifer *Orbulina universa*. *Earth and Planetary Science Letters*, *309*(3), 291–301. https://doi.org/10.1016/j.epsl.2011.07.010

Allen, K. A., Sikes, E. L., Anderson, R. F., & Rosenthal, Y. (2020). Rapid loss of CO_2 from the south Pacific Ocean during the last glacial termination. *Paleoceanography and Paleoclimatology*, *35*(2). https://doi.org/10.1029/2019PA003766

Anderson, R. F., Ali, S., Bradtmiller, L. I., Nielsen, S. H. H., Fleisher, M. Q., Anderson, B. E., & Burckle, L. H. (2009). Wind-driven upwelling in the Southern Ocean and the deglacial rise in atmospheric CO_2. *Science*, *323*(5920), 1443–1448. https://doi.org/10.1126/science.1167441

Aumont, O., & Bopp, L. (2006). Globalizing results from ocean in situ iron fertilization studies: Globalizing iron fertilization. *Global Biogeochemical Cycles*, *20*, GB2017. https://doi.org/10.1029/2005GB002591

Barnola, J. M., Raynaud, D., Korotkevicht, Y. S., & Lorius, C. (1987). Vostok ice core provides 160,000-year record of atmospheric CO_2, *Nature*, 329(6138). https://doi.org/10.1038/329408a0

Bemis, B. E., Spero, H. J., & Thunell, R. C. (2002). Using species-specific paleotemperature equations with foraminifera: A case study in the Southern California Bight. *Marine Micropaleontology*, *46*(3), 405–430. https://doi.org/10.1016/S0377-8398(02)00083-X

Bopp, L., Kohfeld, K. E., Le Quéré, C., & Aumont, O. (2003). Dust impact on marine biota and atmospheric CO_2 during glacial periods. *Paleoceanography*, *18*(2). https://doi.org/10.1029/2002PA000810

Boyle, E. A. (1983). Manganese carbonate overgrowths on foraminifera tests. *Geochimica et Cosmochimica Acta*, *47*(10), 1815–1819. https://doi.org/10.1016/0016-7037(83)90029-7

Brandes, J. A., Devol, A. H., Yoshinari, T., Jayakumar, D. A., & Naqvi, S. W. A. (1998). Isotopic composition of nitrate in the central Arabian Sea and eastern tropical North Pacific: A tracer for mixing and nitrogen cycles. *Limnology and Oceanography*, *43*(7), 1680–1689. https://doi.org/10.4319/lo.1998.43.7.1680

Broecker, W. S. (1982). Glacial to interglacial changes in ocean chemistry. *Progress in Oceanography*, *11*. 151–197. https://doi.org/10.1016/0079-6611(82)90007-6

Broecker, W. S., & Henderson, G. M. (1998). The sequence of events surrounding Termination II and their implications for the cause of glacial-interglacial CO_2 changes. *Paleoceanography*, *13*(4), 352–364. https://doi.org/10.1029/98PA00920

Brovkin, V., Ganopolski, A., Archer, D., & Rahmstorf, S. (2007). Lowering of glacial atmospheric CO_2 in response to changes in oceanic circulation and marine biogeochemistry. *Paleoceanography*, *22*(4). https://doi.org/10.1029/2006PA001380

Calvo, E., Pelejero, C., Pena, L. D., Cacho, I., & Logan, G. A. (2011). Eastern Equatorial Pacific productivity and related-CO_2 changes since the last glacial period. *Proceedings of the National Academy of Sciences*, *108*(14), 5537–5541. https://doi.org/10.1073/pnas.1009761108

Cartapanis, O., Tachikawa, K., & Bard, E. (2011). Northeastern Pacific oxygen minimum zone variability over the past 70 kyr: Impact of biological production and oceanic ventilation. *Paleoceanography*, *26*(4). https://doi.org/10.1029/2011PA002126

Chance, R., Weston, K., Baker, A. R., Hughes, C., Malin, G., Carpenter, L., et al. (2010). Seasonal and interannual variation of dissolved iodine speciation at a coastal Antarctic site. *Marine Chemistry*, *118*(3), 171–181. https://doi.org/10.1016/j.marchem.2009.11.009

Chase, Z., Anderson, R. F., Fleisher, M. Q., & Kubik, P. W. (2002). The influence of particle composition and particle flux on scavenging of Th, Pa and Be in the ocean. *Earth and Planetary Science Letters*, *204*(1), 215–229. https://doi.org/10.1016/S0012-821X(02)00984-6

Close, B. J. (2020). *Constraining Respired Carbon Storage in the Eastern Tropical Pacific over the Last 25 Thousand Years Using Benthic Foraminiferal Boron/Calcium Ratios* (M.S.). *ProQuest Dissertations and Theses*. Old Dominion University, United States -- Virginia. Retrieved from http://search.proquest.com/pqdtlocal1005724/docview/2479666024/abstract/46FE80BFA73B4ECDPQ/1

Dubois, N., Kienast, M., Kienast, S., Normandeau, C., Calvert, S. E., Herbert, T. D., & Mix, A. (2011). Millennial-scale variations in hydrography and biogeochemistry in the Eastern Equatorial Pacific over the last 100 kyr. *Quaternary Science Reviews*, *30*(1–2), 210–223. https://doi.org/10.1016/j.quascirev.2010.10.012

Elderfield, H., & Ganssen, G. (2000). Past temperature and δ 18 O of surface ocean waters inferred from foraminiferal Mg/Ca ratios. *Nature*, *405*(6785), 442–445. https://doi.org/10.1038/35013033

Eguchi, N. O., Kawahata, H., & Taira, A. (1999). Seasonal response of planktonic foraminifera to surface ocean condition: sediment trap results from the central north Pacific Ocean. *Journal of Oceanography*, *55*(6), 681–691. https://doi.org/10.1023/A:1007812028703

Emerson, S., & Hedges, J. (2008). *Chemical Oceanography and the Marine Carbon Cycle*. Cambridge University Press.

Fairbanks, R. G., Sverdlove, M., Free, R., Wiebe, P. H., & Bé, A. W. H. (1982). Vertical distribution and isotopic fractionation of living planktonic foraminifera from the Panama Basin. *Nature*, *298*(5877), 841–844. https://doi.org/10.1038/298841a0

Feely, R. A., Doney, S. C., & Cooley, S. R. (2009). Ocean acidification: Present conditions and future changes in a high-CO_2 world. *Oceanography*, *22*(4), 36-47.

Fiedler, P. C., & Talley, L. D. (2006). Hydrography of the eastern tropical Pacific: A review. *Progress in Oceanography*, *69*(2–4), 143–180. https://doi.org/10.1016/j.pocean.2006.03.008

Foster, G. L. (2008). Seawater pH, pCO_2 and [CO2−3] variations in the Caribbean Sea over the last 130 kyr: A boron isotope and B/Ca study of planktic foraminifera. *Earth and Planetary Science Letters*, *271*(1–4), 254–266. https://doi.org/10.1016/j.epsl.2008.04.015

Francois, R., Frank, M., Loeff, M. M. R. van der, & Bacon, M. P. (2004). ^{230}Th normalization: An essential tool for interpreting sedimentary fluxes during the late Quaternary. *Paleoceanography*, *19*(1). https://doi.org/10.1029/2003PA000939

Gruber, N. (2011). Oceanic sources and sinks of atmospheric CO_2: A scale interaction challenge. In *COST Action 735" Tools for Assessing Global Air-Sea Fluxes of Climate and Air Pollution Relevant Gases" Final Event*. COST Action 735.

Gruber, N., Clement, D., Carter, B. R., Feely, R. A., van Heuven, S., Hoppema, M., et al. (2019). The oceanic sink for anthropogenic CO_2 from 1994 to 2007. *Science*, *363*(6432), 1193–1199. https://doi.org/10.1126/science.aau5153

Hart, T. J. (1934). On the phytoplankton of the southeast Atlantic and the Bellingshausen Sea, 1929-1931. *Discovery Reports*, *8*, 1–268.

Hayes, C. T., Anderson, R. F., & Fleisher, M. Q. (2011). Opal accumulation rates in the equatorial Pacific and mechanisms of deglaciation. *Paleoceanography*, *26*(1). https://doi.org/10.1029/2010PA002008

Heinze, C., Meyer, S., Goris, N., Anderson, L., Steinfeldt, R., Chang, N., et al. (2015). The ocean carbon sink – impacts, vulnerabilities and challenges. *Earth System Dynamics*, *6*(1), 327–358. https://doi.org/10.5194/esd-6-327-2015

Hendy, I. L., & Kennett, J. P. (2000). Dansgaard-Oeschger cycles and the California Current system: Planktonic foraminiferal response to rapid climate change in Santa Barbara Basin, Ocean Drilling Program Hole 893A. *Paleoceanography*, *15*(1), 30–42. https://doi.org/10.1029/1999PA000413

Hönisch, B., & Hemming, N. G. (2005). Surface ocean pH response to variations in pCO_2 through two full glacial cycles. *Earth and Planetary Science Letters*, *236*(1–2), 305–314. https://doi.org/10.1016/j.epsl.2005.04.027

Hoogakker, B. A. A., Lu, Z., Umling, N., Jones, L., Zhou, X., Rickaby, R. E. M., et al. (2018). Glacial expansion of oxygen-depleted seawater in the eastern tropical Pacific. *Nature*, *562*(7727), 410–413. https://doi.org/10.1038/s41586-018-0589-x

Kawahata, H., Nishimura, A., & Gagan, M. K. (2002). Seasonal change in foraminiferal production in the western equatorial Pacific warm pool: evidence from sediment trap experiments. *Deep Sea Research Part II: Topical Studies in Oceanography*, *49*(13–14), 2783–2800. https://doi.org/10.1016/S0967-0645(02)00058-9

Kienast, S. S., Calvert, S. E., & Pedersen, T. F. (2002). Nitrogen isotope and productivity variations along the northeast Pacific margin over the last 120 kyr: Surface and subsurface paleoceanography. *Paleoceanography*, *17*(4), 7-1-7–17. https://doi.org/10.1029/2001PA000650

Kohfeld, K. E., Quéré, C. L., Harrison, S. P., & Anderson, R. F. (2005). Role of marine biology in glacial-interglacial CO_2 cycles. *Science*, *308*(5718), 74–78. https://doi.org/10.1126/science.1105375

Kretschmer, K., Jonkers, L., Kucera, M., & Schulz, M. (2018). Modeling seasonal and vertical habitats of planktonic foraminifera on a global scale. *Biogeosciences*, *15*(14), 4405–4429. https://doi.org/10.5194/bg-15-4405-2018

Krupinski, N. B. Q., Russell, A. D., Pak, D. K., & Paytan, A. (2017). Core-top calibration of B/Ca in Pacific Ocean *Neogloboquadrina incompta* and *Globigerina bulloides* as a surface water carbonate system proxy. *Earth and Planetary Science Letters*, *466*, 139–151. https://doi.org/10.1016/j.epsl.2017.03.007

Lambeck, K. (2001). Sea level change through the last glacial cycle. *Science*, *292*(5517), 679–686. https://doi.org/10.1126/science.1059549

Lea, D. W., Martin, P. A., Pak, D. K., & Spero, H. J. (2002). Reconstructing a 350ky history of sea level using planktonic Mg/Ca and oxygen isotope records from a Cocos Ridge core. *Quaternary Science Reviews*, *21*(1–3), 283–293. https://doi.org/10.1016/S0277-3791(01)00081-6

Lea, D. W., Pak, D. K., & Spero, H. J. (2000). Climate impact of late quaternary equatorial Pacific sea surface temperature variations. *Science*, *289*(5485), 1719–1724. https://doi.org/10.1126/science.289.5485.1719

Loubere, P. (2000). Marine control of biological production in the eastern equatorial Pacific Ocean. *Nature*, *406*(6795), 497–500. https://doi.org/10.1038/35020041

Loveley, M. R., Marcantonio, F., Wisler, M. M., Hertzberg, J. E., Schmidt, M. W., & Lyle, M. (2017). Millennial-scale iron fertilization of the eastern equatorial Pacific over the past 100,000 years. *Nature Geoscience*, *10*(10), 760–764. https://doi.org/10.1038/ngeo3024

Lovenduski, N. S., Long, M. C., & Lindsay, K. (2015). Natural variability in the surface ocean carbonate ion concentration. *Biogeosciences*, *12*(21), 6321–6335. https://doi.org/10.5194/bg-12-6321-2015

Martin, J. H., Coale, K. H., Johnson, K. S., Fitzwater, S. E., Gordon, R. M., Tanner, S. J., et al. (1994). Testing the iron hypothesis in ecosystems of the equatorial Pacific Ocean. *Nature*, *371*(6493), 123–129. https://doi.org/10.1038/371123a0

Martin, John H. (1990). Glacial-interglacial CO_2 change: The iron hypothesis. *Paleoceanography*, *5*(1), 1–13. https://doi.org/10.1029/PA005i001p00001

Martin, John H., Gordon, M., & Fitzwater, S. E. (1991). The case for iron. *Limnology and Oceanography*, *36*(8), 1793–1802. https://doi.org/10.4319/lo.1991.36.8.1793

Martínez-Botí, M. A., Marino, G., Foster, G. L., Ziveri, P., Henehan, M. J., Rae, J. W. B., et al. (2015). Boron isotope evidence for oceanic carbon dioxide leakage during the last deglaciation. *Nature*, *518*(7538), 219–222. https://doi.org/10.1038/nature14155

Martinez, P., & Robinson, R. S. (2010). Increase in water column denitrification during the last deglaciation: the influence of oxygen demand in the eastern equatorial Pacific. *Biogeosciences*, *7*(1), 1–9. https://doi.org/10.5194/bg-7-1-2010

Meyers, S. R. (2007). Production and preservation of organic matter: The significance of iron. *Paleoceanography*, *22*(4). https://doi.org/10.1029/2006PA001332

Monnin, E., Indermühle, A., Dällenbach, A., Flückiger, J., Stauffer, B., Stocker, T. F., et al. (2001). Atmospheric CO2 Concentrations over the Last Glacial Termination. *Science*, *291*(5501), 112–114. https://doi.org/10.1126/science.291.5501.112

Osborne, E. B., Thunell, R. C., Marshall, B. J., Holm, J. A., Tappa, E. J., Benitez-Nelson, C., et al. (2016). Calcification of the planktonic foraminifera *Globigerina bulloides* and carbonate ion concentration: Results from the Santa Barbara Basin. *Paleoceanography*, *31*(8), 1083–1102. https://doi.org/10.1002/2016PA002933

Peacock, S., Lane, E., & Restrepo, J. M. (2006). A possible sequence of events for the generalized glacial-interglacial cycle. *Global Biogeochemical Cycles*, *20*(2). https://doi.org/10.1029/2005GB002448

Pena, L. D., Calvo, E., Cacho, I., Eggins, S., & Pelejero, C. (2005). Identification and removal of Mn-Mg-rich contaminant phases on foraminiferal tests: Implications for Mg/Ca past temperature reconstructions. *Geochemistry, Geophysics, Geosystems*, *6*(9). https://doi.org/10.1029/2005GC000930

Pena, L. D., Cacho, I., Ferretti, P., & Hall, M. A. (2008). El Niño–Southern Oscillation–like variability during glacial terminations and interlatitudinal teleconnections. *Paleoceanography*, *23*(3). https://doi.org/10.1029/2008PA001620

Pennington, J. T., Mahoney, K. L., Kuwahara, V. S., Kolber, D. D., Calienes, R., & Chavez, F. P. (2006). Primary production in the eastern tropical Pacific: A review. *Progress in Oceanography*, *69*(2–4), 285–317. https://doi.org/10.1016/j.pocean.2006.03.012

Pépin, L., Raynaud, D., Barnola, J.-M., & Loutre, M. F. (2001). Hemispheric roles of climate forcings during glacial-interglacial transitions as deduced from the Vostok record and LLN-2D model experiments. *Journal of Geophysical Research: Atmospheres*, *106*(D23), 31885–31892. https://doi.org/10.1029/2001JD900117

Petit, J. R., Jouzel, J., Raynaud, D., Barkov, N. I., Barnola, J.-M., Basile, I., et al. (1999). Climate and atmospheric history of the past 420,000 years from the Vostok ice core, Antarctica. *Nature*, *399*(6735), 429–436. https://doi.org/10.1038/20859

Rae, J. W. B., Foster, G. L., Schmidt, D. N., & Elliott, T. (2011). Boron isotopes and B/Ca in benthic foraminifera: Proxies for the deep ocean carbonate system. *Earth and Planetary Science Letters*, *302*(3–4), 403–413. https://doi.org/10.1016/j.epsl.2010.12.034

Raven, J., Caldeira, K., Elderfield, H., Hoegh-Guldberg, O., Liss, P., Riebesell, U., Shepherd, J., Turley, C. and Watson, A., (2005). *Ocean acidification due to increasing atmospheric carbon dioxide*. The Royal Society.

Raynaud, D., Barnola, J.-M., Souchez, R., Lorrain, R., Petit, J.-R., Duval, P., & Lipenkov, V. Y. (2005). The record for marine isotopic stage 11. *Nature*, *436*(7047), 39–40. https://doi.org/10.1038/43639b

Robinson, R. S., Martinez, P., Pena, L. D., & Cacho, I. (2009). Nitrogen isotopic evidence for deglacial changes in nutrient supply in the eastern equatorial Pacific. *Paleoceanography*, *24*(4). https://doi.org/10.1029/2008PA001702

Sanyal, A., Hemming, N. G., Hanson, G. N., & Broecker, W. S. (1995). Evidence for a higher pH in the glacial ocean from boron isotopes in foraminifera. *Nature*, *373*(6511), 234–236. https://doi.org/10.1038/373234a0

Sautter, L. R., & Thunell, R. C. (1991). Planktonic foraminiferal response to upwelling and seasonal hydrographic conditions; sediment trap results from San Pedro Basin, Southern California Bight. *Journal of Foraminiferal Research*, *21*(4), 347–363. https://doi.org/10.2113/gsjfr.21.4.347

Schmidt, G. A. (1999). Error analysis of paleosalinity calculations. *Paleoceanography*, *14*(3), 422–429. https://doi.org/10.1029/1999PA900008

Schmidt, M. W., Chang, P., Hertzberg, J. E., Them, T. R., Ji, L., & Otto-Bliesner, B. L. (2012). Impact of abrupt deglacial climate change on tropical Atlantic subsurface temperatures. *Proceedings of the National Academy of Sciences*, *109*(36), 14348–14352. https://doi.org/10.1073/pnas.1207806109

Schmittner, A., & Galbraith, E. D. (2008). Glacial greenhouse-gas fluctuations controlled by ocean circulation changes. *Nature*, *456*(7220), 373–376. https://doi.org/10.1038/nature07531

Schneider, C. A., Rasband, W. S., & Eliceiri, K. W. (2012). NIH Image to ImageJ: 25 years of image analysis. *Nature Methods*, *9*(7), 671–675. https://doi.org/10.1038/nmeth.2089

Sigman, D. M., & Boyle, E. A. (2000). Glacial/interglacial variations in atmospheric carbon dioxide. *Nature*, *407*(6806), 859–869. https://doi.org/10.1038/35038000

Somes, C. J., Schmittner, A., & Altabet, M. A. (2010). Nitrogen isotope simulations show the importance of atmospheric iron deposition for nitrogen fixation across the Pacific Ocean. *Geophysical Research Letters*, *37*(23). https://doi.org/10.1029/2010GL044537

Spero, H. J., Bijma, J., Lea, D. W., & Bemis, B. E. (1997). Effect of seawater carbonate concentration on foraminiferal carbon and oxygen isotopes. *Nature*, *390*(6659), 497–500. https://doi.org/10.1038/37333

Spero, H. J., Bijma, J., Lea, D. W., & Russell, A. D. (1999). Deconvolving glacial ocean carbonate chemistry from the planktonic foraminifera carbon isotope record. In F. Abrantes & A. C. Mix (Eds.), *Reconstructing Ocean History* (pp. 329–342). Boston, MA: Springer US. https://doi.org/10.1007/978-1-4615-4197-4_19

Takahashi, T., Sutherland, S. C., Wanninkhof, R., Sweeney, C., Feely, R. A., Chipman, D. W., et al. (2009). Climatological mean and decadal change in surface ocean pCO_2, and net sea–air CO2 flux over the global oceans. *Deep Sea Research Part II: Topical Studies in Oceanography*, *56*(8–10), 554–577. https://doi.org/10.1016/j.dsr2.2008.12.009

Thunell, R. C., & Reynolds, L. A. (1984). Sedimentation of planktonic foraminifera: seasonal changes in species flux in the Panama Basin. *Micropaleontology*, *30*(3), 243. https://doi.org/10.2307/1485688

Tripati, A. K., Roberts, C. D., & Eagle, R. A. (2009). Coupling of CO_2 and ice sheet stability over major climate transitions of the last 20 million years. *Science*, *326*(5958), 1394–1397. https://doi.org/10.1126/science.1178296

Tolderlund, D. S., & Bé, A. W. H. (1971). Seasonal Distribution of Planktonic Foraminifera in the Western North Atlantic. *Micropaleontology*, *17*(3), 297–329. https://doi.org/10.2307/1485143

Tyrrell, T., Merico, A., Waniek, J. J., Wong, C. S., Metzl, N., & Whitney, F. (2005). Effect of seafloor depth on phytoplankton blooms in high-nitrate, low-chlorophyll (HNLC) regions. *Journal of Geophysical Research: Biogeosciences*, *110*(G2). https://doi.org/10.1029/2005JG000041

Tyrrell, Toby, & Zeebe, R. E. (2004). History of carbonate ion concentration over the last 100 million years. *Geochimica et Cosmochimica Acta*, *68*(17), 3521–3530. https://doi.org/10.1016/j.gca.2004.02.018

Umling, N. E., Thunell, R. C., & Bizimis, M. (2018). Deepwater expansion and enhanced remineralization in the eastern equatorial Pacific during the last glacial maximum. *Paleoceanography and Paleoclimatology*, *33*(6), 563–578. https://doi.org/10.1029/2017PA003221

Watson, A. J., Bakker, D. C. E., Ridgwell, A. J., Boyd, P. W., & Law, C. S. (2000). Effect of iron supply on Southern Ocean CO_2 uptake and implications for glacial atmospheric CO2. *Nature*, *407*(6805), 730–733. https://doi.org/10.1038/35037561

Winckler, G., Anderson, R. F., Fleisher, M. Q., McGee, D., & Mahowald, N. (2008). Covariant glacial-interglacial dust fluxes in the equatorial Pacific and Antarctica. *Science*, *320*(5872), 93–96. https://doi.org/10.1126/science.1150595

Wolf-Gladrow, D. A., Zeebe, R. E., Klaas, C., Körtzinger, A., & Dickson, A. G. (2007). Total alkalinity: The explicit conservative expression and its application to biogeochemical processes. *Marine Chemistry*, *106*(1–2), 287–300. https://doi.org/10.1016/j.marchem.2007.01.006

Yu, J., Elderfield, H., & Hönisch, B. (2007). B/Ca in planktonic foraminifera as a proxy for surface seawater pH. *Paleoceanography*, *22*(2). https://doi.org/10.1029/2006PA001347

Yu, J., Foster, G. L., Elderfield, H., Broecker, W. S., & Clark, E. (2010). An evaluation of benthic foraminiferal B/Ca and $\delta^{11}B$ for deep ocean carbonate ion and pH reconstructions. *Earth and Planetary Science Letters*, *293*(1), 114–120. https://doi.org/10.1016/j.epsl.2010.02.029

Zeebe, R. E. (2012). History of seawater carbonate chemistry, atmospheric CO_2, and ocean acidification. *Annual Review of Earth and Planetary Sciences*, *40*(1), 141–165. https://doi.org/10.1146/annurev-earth-042711-105521

Zeebe, R. E., & Wolf-Gladrow, D. (2001). *CO_2 in Seawater: Equilibrium, Kinetics, Isotopes*. Gulf Professional Publishing.

VITA

Lenzie Gail Ward

EDUCATION

2019-Present **M.S.,** Ocean and Earth Science
Old Dominion University, 4402 Elkhorn Avenue, Norfolk, VA
Adviser: Dr. Matthew Schmidt

2016-2019 **B.S.**, Ocean, Earth, and Atmospheric Science (Geology Concentration)
Old Dominion University, 4402 Elkhorn Avenue, Norfolk, VA

PRESENTATIONS & CONFERENCE PROCEEDINGS

2020 **L.G. Ward**, M.W. Schmidt, J.E. Hertzberg, H.J. Spero, and F. Marcantonio. Reconstructing surface water carbonate ion concentration changes in the Eastern Equatorial Pacific across glacial transitions. Oral presentation, AGU Fall Meeting, Virtual, December 2020

2020 **L.G. Ward**, M.W. Schmidt, J.E. Hertzberg, H.J. Spero, and F. Marcantonio. Reconstructing surface water carbonate ion concentration changes in the Eastern Equatorial Pacific across glacial transitions. Poster presentation, GSA Fall Meeting, Virtual, October 2020

2020 **L.G. Ward**, M.W. Schmidt, J.E. Hertzberg, H.J. Spero, and F. Marcantonio. Reconstructing surface water carbonate ion concentration changes in the Eastern Equatorial Pacific using B/Ca ratios in *Globigerina bulloides* over the past 25 kyr. Poster presentation, AGU Fall Meeting, San Francisco, CA, December 2019

2019 **L.G. Ward**, M.W. Schmidt, J.E. Hertzberg, and F. Marcantonio. Reconstructing surface water carbonate ion concentration changes in the Eastern Equatorial Pacific using B/Ca ratios in *Globigerina bulloides* over the past 25 kyr. Poster presentation, Old Dominion University's Undergraduate Research Symposium, February 2019

2018 **L.G. Ward**, M.W. Schmidt, J.E. Hertzberg, and F. Marcantonio. Reconstructing surface water carbonate ion concentration changes in the Eastern Equatorial Pacific using B/Ca ratios in *Globigerina bulloides* over the past 25 kyr. Poster presentation, AGU Fall Meeting, Washington D.C., December 2018

AWARDS, FELLOWSHIPS, & SCHOLARSHIPS

2020 Dorothy Brown Smith Scholarship, Old Dominion University ($100)

2019-2020 Neil & Susan Kelley Endowed Scholarship, Old Dominion University ($4998)

2019 Undergraduate Research & Creativity Grant, Old Dominion University's Honors College ($2000)

2018-2019 C.S. Sherwood III Scholarship, Old Dominion University ($840)

2017-2018 Program for Undergraduate Research & Scholarship (PURS), Old Dominion University's Honors College ($10,000)